Resource

Cell Reports

A Multi-layered Quantitative *In Vivo* Expression Atlas of the Podocyte Unravels Kidney Disease Candidate Genes

Graphical Abstract

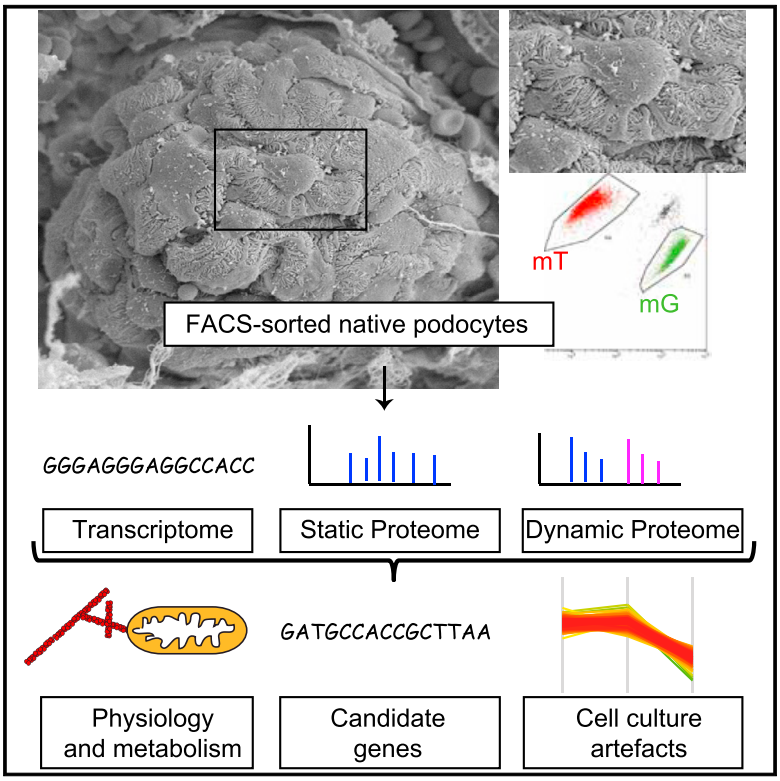

Highlights

- Deep proteome and transcriptome analyses of native podocytes unravel druggable targets
- Static and dynamic proteomics uncover features of podocyte identity and proteostasis
- Candidate genes for nephrotic syndrome were predicted based on multi-omic integration
- FARP1 is a previously unreported candidate gene for human proteinuric kidney disease

Authors

Markus M. Rinschen, Markus Gödel, Florian Grahammer, ..., Joern Dengjel, Thomas Benzing, Tobias B. Huber

Correspondence

markus.rinschen@uk-koeln.de (M.M.R.), thomas.benzing@uk-koeln.de (T.B.), t.huber@uke.de (T.B.H.)

In Brief

The podocyte forms the most outer and essential part of the renal filter and restricts the passage of proteins from blood to urine. Rinschen et al. combine deep proteomic and transcriptomic data with protein dynamics from native mouse podocytes to reveal insights into podocyte biology and to identify candidate disease genes.

Rinschen et al., 2018, Cell Reports *23*, 2495–2508
May 22, 2018
https://doi.org/10.1016/j.celrep.2018.04.059

CellPress

Cell Reports
Resource

A Multi-layered Quantitative *In Vivo* Expression Atlas of the Podocyte Unravels Kidney Disease Candidate Genes

Markus M. Rinschen,[1,2,3,4,23,*] Markus Gödel,[5,6,23] Florian Grahammer,[5,6,23] Stefan Zschiedrich,[6] Martin Helmstädter,[6] Oliver Kretz,[5,6] Mostafa Zarei,[8,9] Daniela A. Braun,[10] Sebastian Dittrich,[1,2] Caroline Pahmeyer,[1,2] Patricia Schroder,[11,12] Carolin Teetzen,[6] HeonYung Gee,[12,13] Ghaleb Daouk,[10] Martin Pohl,[14] Elisa Kuhn,[15] Bernhard Schermer,[1,2,3,4] Victoria Küttner,[7,8,16] Melanie Boerries,[17,18,19] Hauke Busch,[17,20] Mario Schiffer,[11,12] Carsten Bergmann,[6,15] Marcus Krüger,[2,3] Friedhelm Hildebrandt,[10] Joern Dengjel,[8,9,16,21,22] Thomas Benzing,[1,2,3,4,24,*] and Tobias B. Huber[5,6,8,9,22,24,25,*]

[1]Department II of Internal Medicine, University of Cologne, 50931 Cologne, Germany
[2]Center for Molecular Medicine Cologne (CMMC), University of Cologne, 50931 Cologne, Germany
[3]Cologne Excellence Cluster on Cellular Stress Responses in Aging Associated Diseases (CECAD), University of Cologne, 50931 Cologne, Germany
[4]Systems Biology of Ageing Cologne (Sybacol), University of Cologne, 50931 Cologne, Germany
[5]III. Department of Medicine, University Medical Center Hamburg-Eppendorf, 20246 Hamburg, Germany
[6]Department of Medicine IV, Medical Center and Faculty of Medicine, University of Freiburg, 79110 Freiburg, Germany
[7]Department for Neuroanatomy, University of Freiburg, 79104 Freiburg, Germany
[8]Freiburg Institute for Advanced Studies (FRIAS), University of Freiburg, 79104 Freiburg, Germany
[9]Center for Systems Biology (ZBSA), Albert Ludwigs University, 79104 Freiburg, Germany
[10]Division of Nephrology, Boston Children's Hospital, Harvard Medical School, Boston, MA 02115, USA
[11]Department of Medicine/Nephrology, Hannover Medical School, 30625 Hannover, Germany
[12]Mount Desert Island Biological Laboratory, Salisbury Cove, ME 04609, USA
[13]Department of Pharmacology, Brain Korea 21 PLUS Project for Medical Sciences, Yonsei University College of Medicine, Seoul 03722, Korea
[14]Department of General Pediatrics, Adolescent Medicine and Neonatology, Medical Center and Faculty of Medicine, University of Freiburg, 79106 Freiburg, Germany
[15]Center for Human Genetics, Bioscientia, 55218 Ingelheim, Germany
[16]Department of Dermatology, Medical Center – University of Freiburg, 79106 Freiburg, Germany
[17]Systems Biology of the Cellular Microenvironment Group, Institute of Molecular Medicine and Cell Research, Albert Ludwigs University Freiburg, 79106 Freiburg, Germany
[18]German Cancer Consortium (DKTK), 79106 Freiburg, Germany
[19]German Cancer Research Center (DKFZ), 69120 Heidelberg, Germany
[20]Lübeck Institute for Experimental Dermatology (LIED), University of Lübeck, 23562 Lübeck, Germany
[21]Department of Biology, University of Fribourg, 1700 Fribourg, Switzerland
[22]BIOSS Centre for Biological Signaling Studies, Albert Ludwigs University Freiburg, 79104 Freiburg, Germany
[23]These authors contributed equally
[24]Senior author
[25]Lead Contact
*Correspondence: markus.rinschen@uk-koeln.de (M.M.R.), thomas.benzing@uk-koeln.de (T.B.), t.huber@uke.de (T.B.H.)
https://doi.org/10.1016/j.celrep.2018.04.059

SUMMARY

Damage to and loss of glomerular podocytes has been identified as the culprit lesion in progressive kidney diseases. Here, we combine mass spectrometry-based proteomics with mRNA sequencing, bioinformatics, and hypothesis-driven studies to provide a comprehensive and quantitative map of mammalian podocytes that identifies unanticipated signaling pathways. Comparison of the *in vivo* datasets with proteomics data from podocyte cell cultures showed a limited value of available cell culture models. Moreover, *in vivo* stable isotope labeling by amino acids uncovered surprisingly rapid synthesis of mitochondrial proteins under steady-state conditions that was perturbed under autophagy-deficient, disease-susceptible conditions. Integration of acquired omics dimensions suggested FARP1 as a candidate essential for podocyte function, which could be substantiated by genetic analysis in humans and knockdown experiments in zebrafish. This work exemplifies how the integration of multi-omics datasets can identify a framework of cell-type-specific features relevant for organ health and disease.

INTRODUCTION

Diseases involving glomeruli, the filtration units of the kidney, are a leading cause of chronic kidney disease (CKD), which affects approximately 15% of all Americans (Meguid El Nahas and Bello,

2005; CDC) and substantially increases cardiovascular events. Despite recent advances in the understanding of glomerular biology, treatment of these disorders has remained extraordinarily challenging in many cases. The podocyte is a postmitotic, neuron-like shaped epithelial cell with limited capacity for self-renewal. Podocytes are essential to maintain a physiological blood-urine barrier (Pavenstädt et al., 2003), and deterioration of podocyte function and subsequent proteinuria are critical accelerators of renal functional decline in disease states. Because of considerable metabolic and mechanical stress, the podocyte needs to maintain its proteome—a prerequisite to maintain its architecture, cytoskeletal integrity, signal transduction, and metabolic function. Interference with any of these functions—for instance, as an inherited gene defect in humans (Boute et al., 2000; Kaplan et al., 2000; Kestilä et al., 1998; Reiser et al., 2005)—leads to proteinuria, podocyte loss, glomerular scarring and, ultimately, chronic kidney disease.

Despite recent progress in the understanding of genetics and signaling of proteinuric kidney disease, the molecular identity of the podocyte is not defined, and it is unclear how its function could be targeted therapeutically. Abundant information regarding podocyte mRNA expression patterns has been gathered recently (Brunskill et al., 2011; Fu et al., 2016; Kann et al., 2015), and integrative genomic studies have enormous potential in classifying human podocyte disease and pathophysiology (Hodgin et al., 2013; Ju et al., 2012; Sampson et al., 2015; Susztak, 2014). However, several studies from different fields found that absolute abundances of mRNA and protein abundances correlate only moderately. Indeed, transcript levels can only explain one- to two-thirds of protein levels, underlining the importance of post-transcriptional control (Liu et al., 2016; Vogel and Marcotte, 2012). In recent years, it became feasible to investigate the entity of proteins, the proteome, at an unprecedented depth (Mann et al., 2013). As a result, proteins can be resolved and quantified relatively and absolutely, culminating in a near-comprehensive mass spectrometry-based expression map of the human proteome (Kim et al., 2014; Wilhelm et al., 2014). In addition, *in vivo* stable amino acid isotope labeling strategies opened new avenues for the quantification of protein dynamics when used in pulse experiments (Krüger et al., 2008; Savas et al., 2012; Toyama et al., 2013). The aim of this study was to generate a quantitative and integrative map of the podocyte proteome, both static and dynamic, and its transcriptome to gain novel and unbiased insights into podocyte biology. To demonstrate the applications of this "atlas," we conducted orthogonal hypothesis-driven studies that supported the presence of unanticipated molecular mechanisms maintaining podocyte protein homeostasis and function.

RESULTS

Absolute Quantification of the Native Podocyte Proteome

GFP-positive mouse podocytes and tomato-positive non-podocyte glomerular cells were isolated from native glomeruli of an hNPHS2Cre*mT/mG mouse using fluorescence-activated cell sorting (FACS) (Boerries et al., 2013). Podocytes expressed GFP, whereas all other viable glomerular non-podocyte cells expressed tomato red fluorescent protein (Figure 1A). A work flow for "deep mapping" of transcriptome, proteome, and proteome dynamics was applied to both podocytes and non-podocytes (Kulak et al., 2014). Quality control of the dataset demonstrated a clear separation between both samples (Figure S1). This approach identified, in total, more than 9,000 different proteins (Tables S1 and S2). We performed absolute quantification of 6,979 proteins using the intensity-based absolute quantification (iBAQ) approach (Table S2). This proteomics parameter is relative to copy numbers in a given sample (Kohli et al., 2014; Schwanhäusser et al., 2011). Cytoskeletal proteins were highly represented in the dataset (Figure 1A). The dynamic range of the podocyte proteome copy numbers comprises seven orders of magnitude (Figure 1B). We mapped genes associated with focal segmental glomerular sclerosis or hereditary nephrotic syndrome on this dataset (Figure 1C; top 10 genes in Figure 1D; Bierzynska et al., 2015). These "disease-associated genes," although only comprising 35 of 7,000 (0.5%) absolutely quantified proteins, contributed approximately 4% of the podocyte protein mass, with cytoskeletal proteins like Actn4 and Arhgdia contributing most to this amount (Figure 1D). Several other known podocyte genes (e.g., Trpc6) were identified but could not be quantified because of their low abundance. To estimate the absolute protein quantity based on the data and determine protein concentrations or copy numbers per cell, we applied a recently developed algorithm on our dataset ("proteomic ruler") (Wiśniewski et al., 2014). This provides a starting point to determine the stoichiometries of known protein complexes; for example, the prominent transmembrane slit diaphragm complex within native mouse podocytes, which comprises podocin-Neph1-Nephrin-Fat1 with a copy number ratio of ~10:2:1:0.5 (Figure 1E), indicating that podocin is by far the most abundant slit diaphragm protein within podocytes (Grahammer et al., 2013).

Integration of Deep Transcriptomic and Proteomics Data

Protein abundance is determined by the rate of transcription but also a result of protein stability and posttranslational processing. To identify the determinants of podocyte protein copy number abundance, we performed comparison with a transcriptomic copy number analysis performed by mRNA sequencing. Our dataset was similar to previously published mRNA sequencing (mRNA-seq) analyses but demonstrated a greater depth upon analysis with the same parameters (Figure 2A; Table S3; Figure S2). Enrichment analyses demonstrated overrepresentation of several known pathways enriched on mRNA levels, among these extracellular matrix (ECM) synthesis and nephrin interactions (Figure 2B; Figures S2E–S2I; Brunskill et al., 2011). To unravel the correlation of transcriptomic data with proteomic data as a whole, iBAQ data were correlated with the transcriptomic (tpm) values, but the correlation was rather weak (Figure 2C). The correlation was stronger for podocytes compared with non-podocytes (Figure 2D). We checked which proteins were specifically stabilized or destabilized posttranscriptionally using 2D enrichment (Cox and Mann, 2012). This algorithm can be used to visualize statistically significant distributions of protein annotations in a 2D space between different "omics" datasets

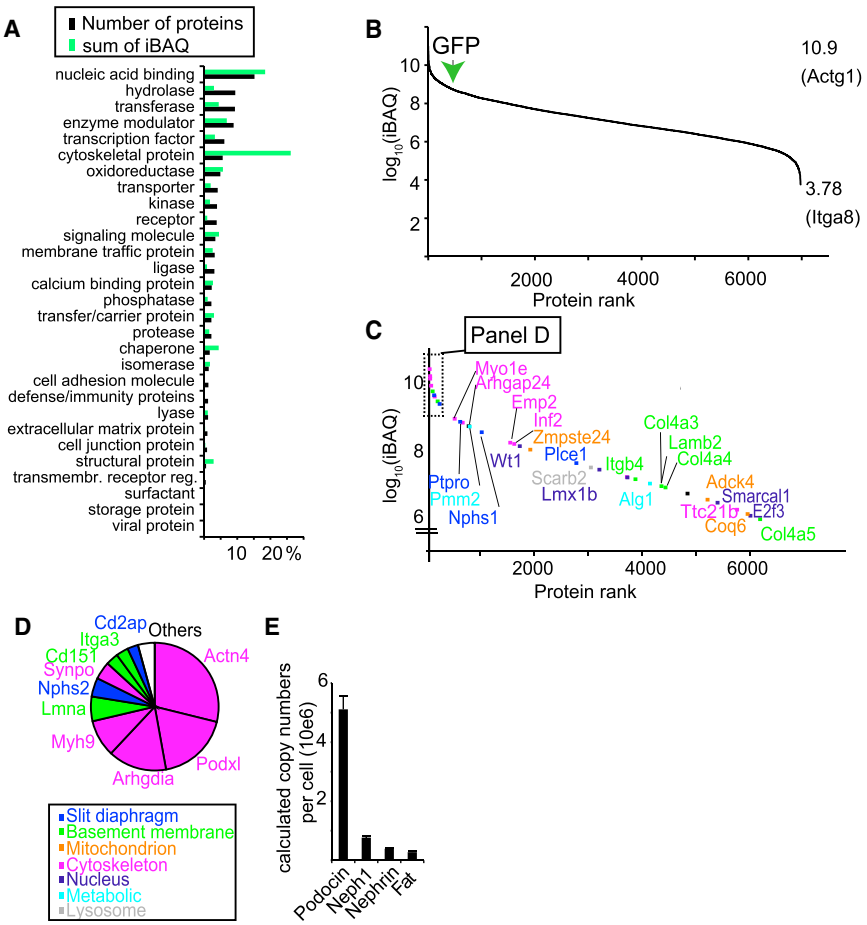

Figure 1. Absolute Quantification of the Native Podocyte Proteome

(A) Panther term analysis of expressed genes and absolute copy numbers (intensity-based absolute quantification [iBAQ]). iBAQ values corresponding to the number of protein copies (green) and the number of different proteins (black) are plotted.

(B) Overview of the dynamic range of the podocyte proteome absolutely quantified using iBAQ.

(C) Expression of proteins encoded by genes causing hereditary nephrotic syndrome and focal segmental glomerulosclerosis in podocytes according to Bierzynska et al. 2015).

(D) Abundance of the 10 most abundant proteins.

(E) Application of the proteomic ruler to detect protein copy numbers of transmembrane proteins of the slit diaphragm complex (Wiśniewski et al., 2014). Calculated numbers of protein copies per cell are depicted.

(Cox and Mann, 2012). The analysis revealed that ECM protein expression was decreased as expected by the respective mRNA expression, which would be expected because of loss of podocyte-produced ECM proteins excreted as part of the glomerular basement membrane assembly (Figure 2E, blue). Proteins involved in controlling metabolism were largely stabilized (Figure 2E, magenta, green). These proteins included glycolysis gene products and proteins involved in amino acid biosynthesis.

Determination of Podocyte-Enriched Proteins

Most of the genes mutated in genetic forms of proteinuria or nephrotic syndrome encode for podocyte-enriched genes. Therefore, we next analyzed whether we could expand the list of known podocyte-enriched proteins compared with other glomerular cells. Using stringent statistical cutoff values for quantification, we found 551 podocyte-enriched proteins (Figure 3A; Table S2); among these were many gene products currently known to be associated with hereditary nephrotic syndrome (Sadowski et al., 2015). Figures S3 and S4A depict standardized stainings of 190 proteins that have a "medium" or "high" staining intensity in the human protein atlas (Uhlén et al., 2015). A systematic Medline search of these 190 proteins revealed that the majority were not explicitly linked to podocytes (Table S4). We performed statistical enrichment for overrepresentation of protein domains in all 551 proteins enriched in podocytes (Figure 3B). Significantly enriched protein domains were Fn3 and immunoglobulin G (IgG)-like domains (e.g., in Nephrin), PDZ domains (e.g., in ezrin and Par-3), i-set domains (e.g., in nephrin and VCAM/NCAM), CH domain (e.g., in actinin-4), and FERM domain proteins (e.g., in ezrin) or tetraspanins (e.g., CD151). On a global level, podocyte-specific proteins were significantly reduced for mitochondria as well as RNA and DNA binding proteins (Figure 3C) and enriched for signaling receptors, cytoskeleton-associated proteins, GTPase-associated proteins, membrane proteins, and (phospho)lipid-modifying proteins (Figure 3D).

To demonstrate that this resource may be used to find essential podocyte proteins, we analyzed the effect of knockdown of one candidate podocyte-enriched gene in *Drosophila* nephrocytes, an established model of podocyte function (Weavers et al., 2009; Zhang et al., 2013). We knocked down Tsp26A, the *Drosophila* homolog of TSP5 and TSP15, two newly identified podocyte-enriched proteins that are representatives of the protein class of tetraspanins (Figure 3D). This resulted in significantly decreased ANF-RFP uptake, indicating loss of filtration function (Figure 3E). We also found overt alterations in nephrocyte ultrastructure (Figure 3F), proving the importance of the tetraspanin protein class for nephrocyte function.

Podocyte protein homeostasis largely depends on signaling mediated via posttranslational modifications, such as phosphorylation, ubiquitylation, acetylation, and proteolytic processing (New et al., 2014). Pinpointing podocyte-specific signaling molecules could help us to understand podocyte physiology and target podocyte signaling pharmacologically or genetically. Table 1 summarizes unanticipated observations of signaling molecules enriched in mouse podocytes; among these were

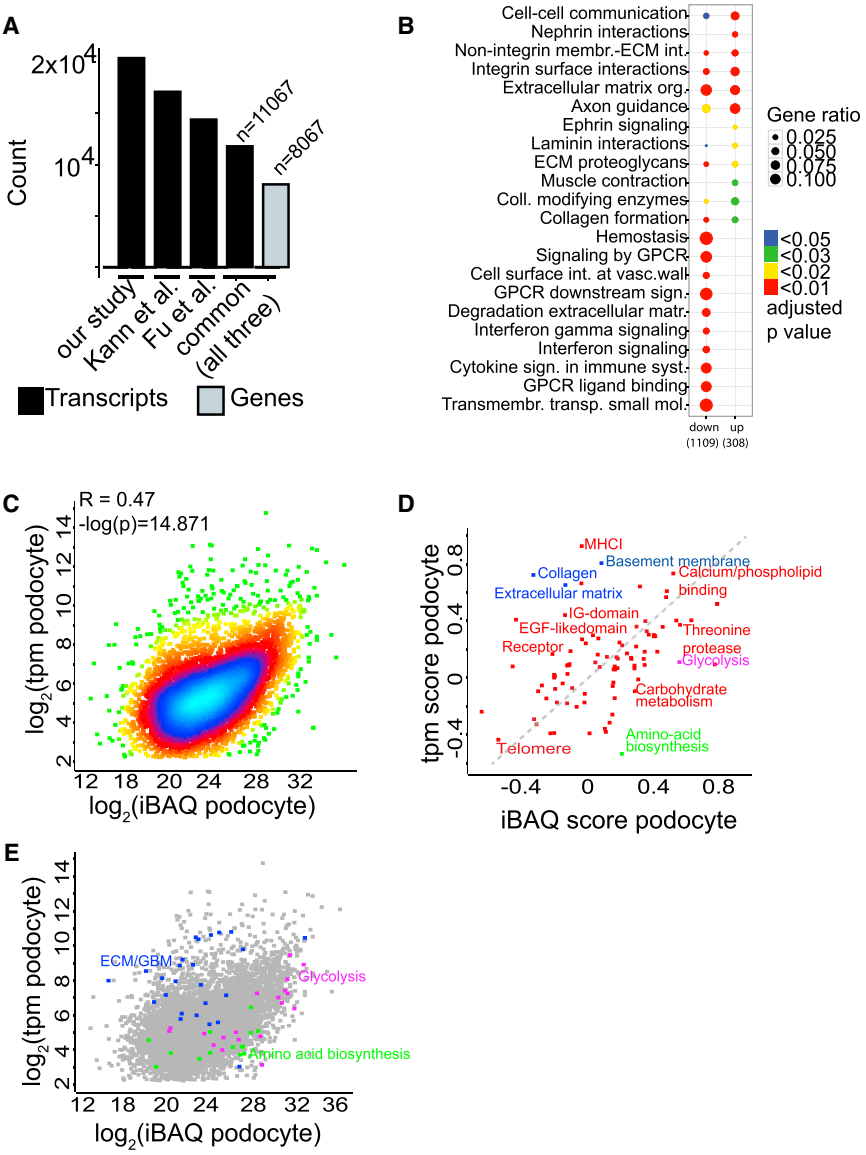

Figure 2. Integration of Deep Transcriptomic and Proteomics Data

(A) Comparison of this and other recent transcriptomic (tpm) studies using mRNA-seq. All datasets were processed with the same bioinformatics pipeline as indicated in the Experimental Procedures.

(B) Reactome analysis of transcripts enriched in podocytes (up) and de-enriched in podocytes (down).

(C) Scatterplot demonstrating correlation between proteomic (iBAQ) and (tpm) copy numbers in podocytes (Pearson's R = 0.47, log(p) = 14.8). The density of individual proteins is color-coded (blue, high density; green, low density).

(D) 2D Uniprot keyword analysis of podocyte transcript and protein copy numbers identifies significantly changed Uniprot keywords with an especially high increase in either omic dataset (permutation-based FDR < 0.05). The dashed gray line (y = x) indicates annotations equally represented in both omic datasets.

(E) Distribution of individual Uniprot keyword members in the original scatterplot (analog to C).

several druggable molecules. (For a full list of podocyte enriched kinases, phosphatases, ubiquitin ligases, proteases, signaling receptors, actin binding proteins and transcription factors, see Table S5). We also mapped the 551 podocyte-enriched proteins against known protein interaction databases to obtain a network and central nodes among these podocyte-enriched proteins (Cerami et al., 2010). The proteins RhoA, Actin, and Grb and the nephrin-regulating kinase Src had most edges within these networks (Figure S4B); all four have reported relevance for podocyte biology (Harita et al., 2008; New et al., 2014; Schmieder et al., 2004), suggesting a central role for these proteins.

Comparison of the Deep Native Podocyte Proteome with the Cultured Podocyte Proteome

We asked whether this unique obtained podocyte proteome resource would help us to investigate the strengths and weaknesses of *in vitro* immortalized podocyte cell cultures, a commonly used tool in podocyte research. To this end, we compared the dataset with a similar, previously published deep quantitative proteomic mapping of a mouse podocyte cell line (Rinschen et al., 2016b). We could identify 6,193 proteins in both samples, representing a significant overlap between both samples (Figure S4C). Clustering analysis of normalized expression values revealed significant differences between native podocytes and the *in vitro* cell line irrespective of the differentiation status (33°C = undifferentiated or 37°C = differentiated; Figure S4D). Clustering analysis revealed eight major clusters. Three clusters contained proteins with high abundance in cell lines compared with the native podocytes and were enriched for proteins related to the actin cytoskeleton, including stress fibers and focal adhesion proteins (Figure 4A). Three clusters contained proteins with low abundance in cell lines compared with the native podocytes (Figure 4B). These clusters were related to phospholipid metabolism and tight junctions. Two clusters showed differences between 33°C and 37°C and native cells; these were, as expected (Rinschen et al., 2016b), related to the cell cycle (Figure 4C). Moreover, disease-causing proteins such as nephrin and podocin or podocyte markers such as WT1 were not at all or only very weakly expressed in podocytes in culture compared with the *in vivo* dataset.

This comparison of podocyte proteomes from cell culture and from native tissue suggested that podocyte cell cultures have an increased abundance of stress fiber-associated proteins and

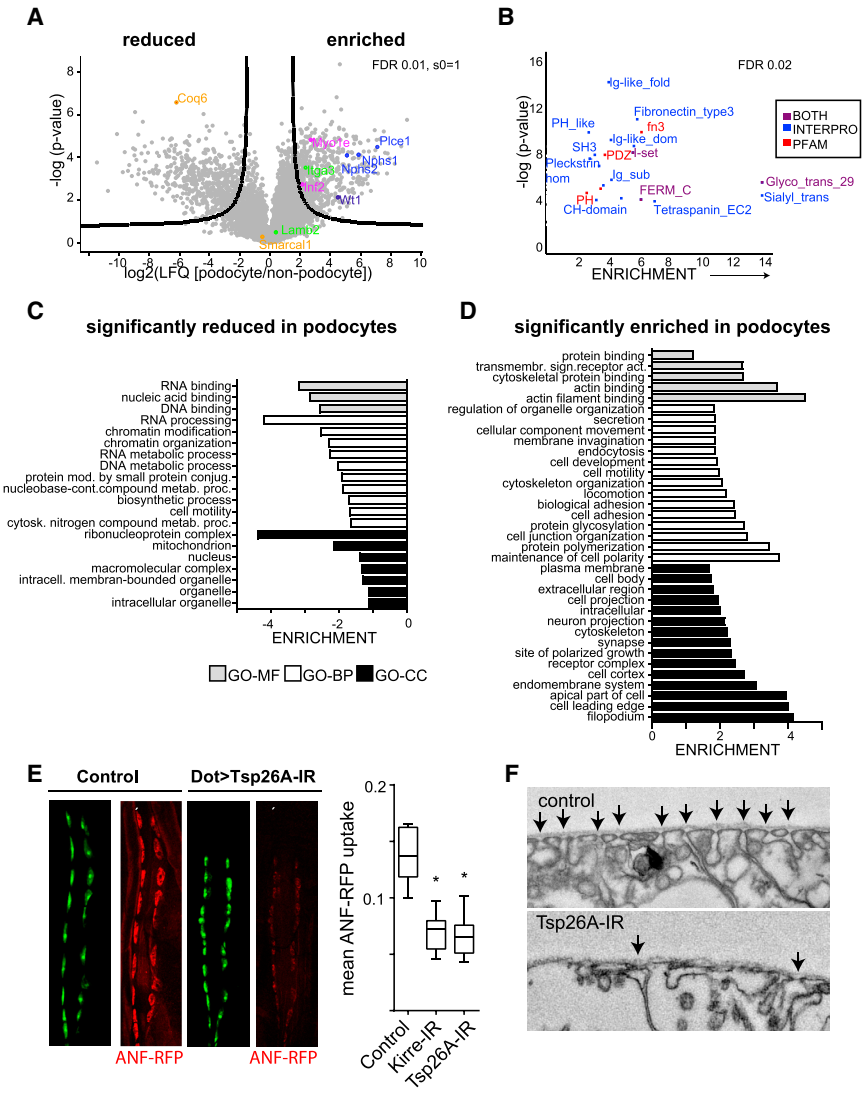

Figure 3. Determination of Podocyte-Enriched Proteins Uncovers Druggable Targets and Candidate Genes for Podocyte Function

(A) Volcano plot of protein quantification of podocytes over non-podocytes. The logarithmic fold change of label-free quantification intensities (LFQs) is plotted versus the negative decadic logarithm of the p value. 551 proteins pass the criteria for significant podocyte enrichment (significance analysis of microarrays [SAM] analysis, s0 = 1, FDR = 0.01).

(B) Enrichment analysis of protein domains in podocytes. Protein domains (PFAM and INTERPRO annotation) were tested for enrichment within the podocyte-enriched proteins over the proteins not significantly enriched. –log(p value) of every significantly enriched protein domain is plotted against fold enrichment. Fisher's exact test, FDR < 0.02.

(C) GO terms overrepresented in the 551 podocyte-enriched proteins compared with non-podocyte specific proteins. Fold enrichment of GO terms representing molecular function (GOMF, gray bars), cellular component (GOCC, black bars), and biological process (GOBP, white bars). All GO terms are statistically enriched in the dataset compared with non-podocyte proteins. Fishers exact test, FDR < 0.05.

(D) Significantly de-enriched GO terms in the 551 podocyte-specific proteins (the same statistical criteria and color code as in C).

(E) CLSM micrographs of pericardial nephrocytes at second larval stage. RNAi-mediated knockdown of Tsp26A significantly reduced ANF-RFP (red) uptake, suggesting that Tsp26A is required for pericardial nephrocyte (green) function. The ANF-RFP uptake is significantly reduced by the knockdown of Tsp26A (p value < 0.05)

(F) Ultrastructural alteration of Tsp26A knockdown nephrocytes. Arrows indicate nephrocyte cell contacts.

focal adhesions. We postulated that some of these differences may have been a cell culture artefact because of the mechanical properties of the plastic dish on which these cells were cultivated. As a proof of principle, we cultured podocytes on soft matrix with an elastic modulus of 12 kPa and compared their proteome with podocytes grown in plastic dishes (in the range of gigapascals). This elastic modulus ("stiffness") of 12 kPa is similar to that of a skeletal muscle cell, a mechanically challenged cell (Gilbert et al., 2010; Janmey and Miller, 2011). Using quantitative proteomics, we found vast differences in the podocyte proteome depending on the matrix on which they were grown (Figures S5A and S5B). On a global level, actin filament proteins and stress fiber proteins were significantly depleted by culturing podocytes on the "soft" matrix, which made them, in this regard, "more similar" to the native podocyte (based on the log2 ratio of podocyte/non-podocyte protein expression) (Figure 4D). A similar picture arose when human podocytes were cultured on soft matrices. The changes in the proteome were larger (Figure S5), and the analysis confirmed again the loss of stress fiber protein expression on the soft matrices (Figure 4E; p and false discovery rate (FDR) < 0.05 in a Fisher's exact test).

Analysis of Podocyte Proteome Dynamics and Integration with Deep Proteomics Mapping

To conclude, our data quantitatively describe expression levels in the podocyte proteome. However, these data did not yet cover an important, rather unexploited component of global proteostasis regulation *in vivo*: the dynamic synthesis and turnover of proteins. To approach this, we used a mouse model of *in vivo* stable isotope labeling (Table S6). To this end, adult mice (10 weeks of age) were fed for 1, 2, and 3 weeks with a diet exclusively containing heavy isotope-labeled lysine. The incorporation of this essential amino acid should correlate with the dynamic synthesis rate (although these data do not strictly correlate with a protein "half-life" because of intracellular amino acid recycling (Krüger

Table 1. Examples of Podocyte-Enriched Kinases, Transcription Factors, and Potentially Druggable Targets

Gene Symbol	Uniprot ID	Log2(Ratio), (−log(p))	Name	Comment	References
Csnk1g3	Q8C4X2	2.14 (2.84)	casein kinase 1 gamma 3	an acidophilic S/T protein kinase that is a candidate for abundant acidophilic phosphorylation on slit diaphragm proteins (Nephrin, Trpc6, and Cd2ap)	Rinschen et al., 2014, 2015b
Nek1	B7ZWK0	3.43 (3.61)	serine/threonine protein kinase Nek1	a protein kinase (STY) responsible for ciliogenesis	Shalom et al., 2008
Mst4	Q99JT2;	2.89 (4.70)	serine/threonine protein kinase MST4	members of the canonical hippo pathway, linked to mechanotransduction and apoptosis, druggable	Schwartzman et al., 2015, Rinschen et al., 2017
Lats2	Q7TSJ6	3.25 (2.37)	serine/threonine protein kinase LATS2		
Tead1	P30051	3.70 [1.83]	transcriptional enhancer factor TEF-1		
Dach1	Q9QYB2	4.63 (4.22)	dachshund homolog 1	a transcription factor strongly enriched in podocytes (comparable with WT1), GWAS demonstrate association with GFR	Köttgen et al., 2010
Cblb	B9EKI5; Q3TTA7	4.10 (2.23)	E3 ubiquitin-protein ligase CBL-B	strongest enriched ubiquitin ligase in podocytes, localizes in immune cells and mediates the expression of EGF receptors in a protein complex with the recently discovered podocin-associated ubiquitin ligase Ubr4, potentially druggable	Rinschen et al., 2016a, Tong et al., 2014, Wirnsberger et al., 2016
Npr3	P70180	4.89 (1.89)	atrial natriuretic peptide receptor 3	mediates ANP signaling via cGMP, confirmation of *in vitro* and *in vivo* studies	Rinschen et al., 2016b, Staffel et al., 2016
Npr1	P18293	2.38 (3.70)	atrial natriuretic peptide receptor 1		
Pth1r	P41593	6.19 (2.78)	PTH receptor	mediates Pth signaling via cAMP, confirmation of *in vitro* studies	Endlich and Endlich, 2002
Ifngr1	P15261	3.85 (1.86)	interferon gamma receptor 1	confirmation of *in vitro* and *in vivo* study, druggable	Gurkan et al., 2013
Mertk	Q60805	4.83 (4.36)	tyrosine protein kinase Mer	most enriched tyrosine kinase family, involved in cancer and development, druggable	Lee-Sherick et al., 2015, Zhang et al., 2014, Fleuren et al., 2014
Tyro3	P55144	4.30 (3.76)	tyrosine protein kinase receptor TYRO3		
Axl	Q6PE80	4.02 (3.32)	Tyrosine-protein kinase receptor UFO		

Log2(Ratio) is defined as log2(LFQ in podocytes)/(LFQ in non-podocytes) and is a measurement of podocyte enrichment. Table S5 gives an overview of each class of the annotated signaling molecules. GWAS, genome-wide association study; EGF, epidermal growth factor; cAMP, cyclic AMP; GFR, glomerular filtration rate; cGMP, cyclic GMP; PTH, parathyroid hormone; atrial natriuretic peptide (ANP).

et al., 2008)). Still, proteins synthesized rapidly should exhibit a high heavy amino acid incorporation rate (and a high heavy/light [H/L] ratio), whereas stable, "long-lived" proteins with slow translation should have a lower incorporation rate (Savas et al., 2012). To see which proteins incorporate isotopes at a similar speed, we performed hierarchical clustering of H/L ratios over the labeling time course. This analysis revealed four major clusters of proteins (Figures 5A and 5B). Gene ontology (GO) term analysis of these four clusters revealed that endoplasmic reticulum (ER)-associated proteins (cluster 4) were particular "dynamic" compared with the nuclear proteins, in particular histones (cluster 1), which only showed minimal increases in the H/L ratio (Figure 5C), consistent with previous studies (Toyama et al., 2013). There was almost no correlation between iBAQ values and H/L ratios (correlation coefficient [R^2] = −0.01) (Fig. S6A).

When comparing podocyte H/L ratios with those of co-sorted non-podocyte cells, we observed that podocyte proteins incorporated more slowly than the parallel sorted non-podocyte cells (Figure 5D). 2D GO analysis revealed that cytoskeletal and mitochondrial proteins had a particularly high protein turnover in podocytes compared with non-podocyte cells (Figure 5E). We also analyzed an intact whole kidney protein sample from an

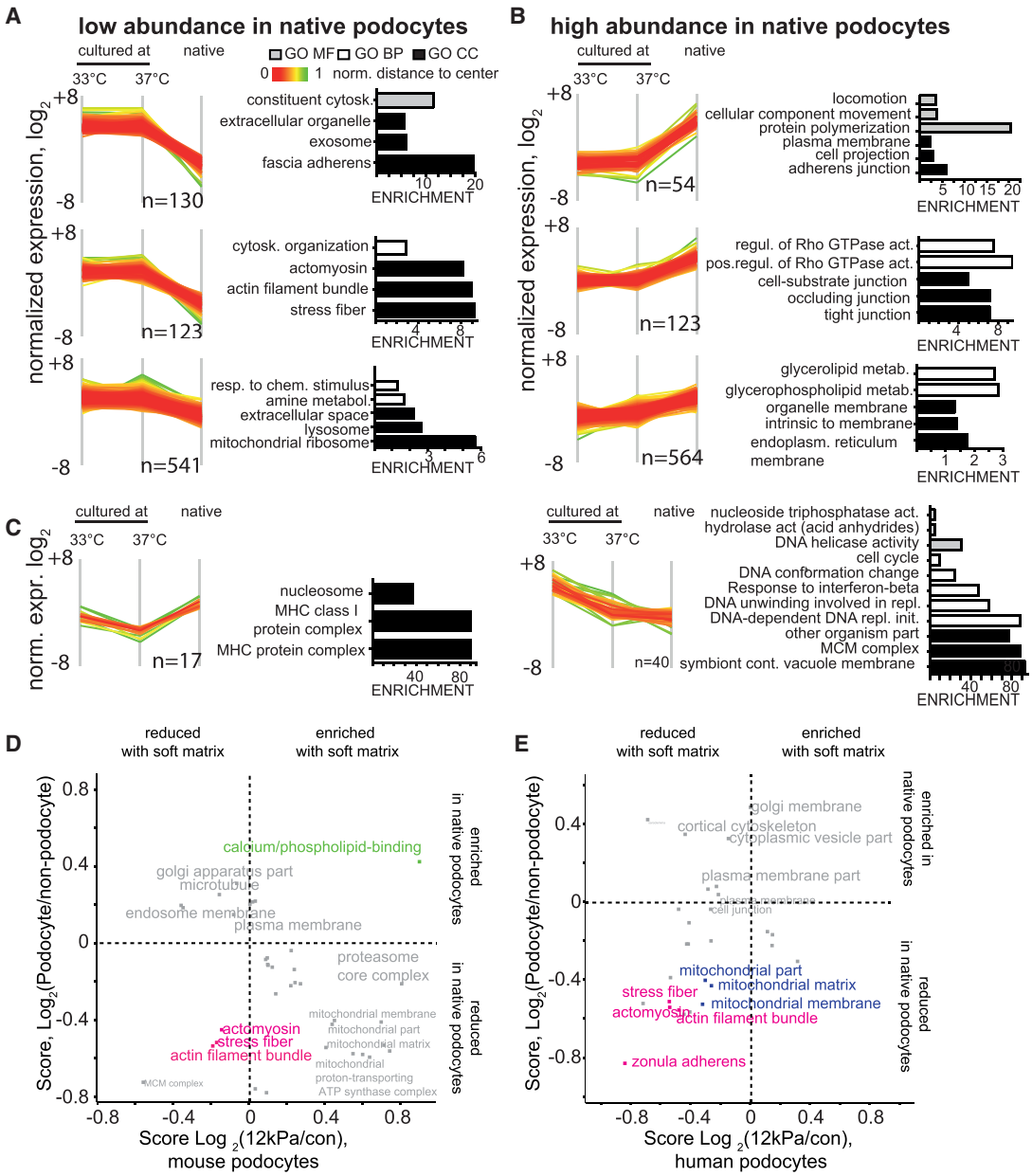

Figure 4. Comparison of the Deep Native (Isolated from Living Mice) and Cultured Podocyte Proteome Enables Functional Analysis of Cell Culture-Induced Proteome Artefacts

(A) Protein clusters were defined based on normalized intensities as depicted in Figure S4C–D. Shown are clusters that have a higher intensity in cultured podocytes compared with the native podocyte proteome. Distance to the mean is color-coded in each cluster. GO terms significantly overrepresented in each cluster are depicted (Fishers exact test, p values corrected with FDR < 0.05).

(B) Three clusters have a lower intensity (and abundance) in the podocyte proteome compared with the cultured podocyte proteome. GO terms significantly overrepresented in each cluster are depicted.

(C) Two clusters have different intensities in undifferentiated and differentiated podocytes.

(D) Mouse podocytes were seeded on matrices with 12 kPa, and the proteome was compared with control cell culture dishes. See Figure S5 for details regarding the dataset. The 2D GO enrichment score of fold change on soft matrix (log2 12 kPa/control) cell culture is plotted against the score for podocyte-enrichment (log2(podocyte/non-podocyte)) (Figure 3). The data demonstrate a significant decrease of stress fiber proteins under both conditions (soft versus stiff matrix and native podocyte versus non-podocyte). Significantly changed terms are plotted (FDR < 0.05)

(E) Human podocytes were seeded on matrices with 12 kPa, and the proteome was compared with control cell culture dishes. See Figure S5 for details regarding the dataset.

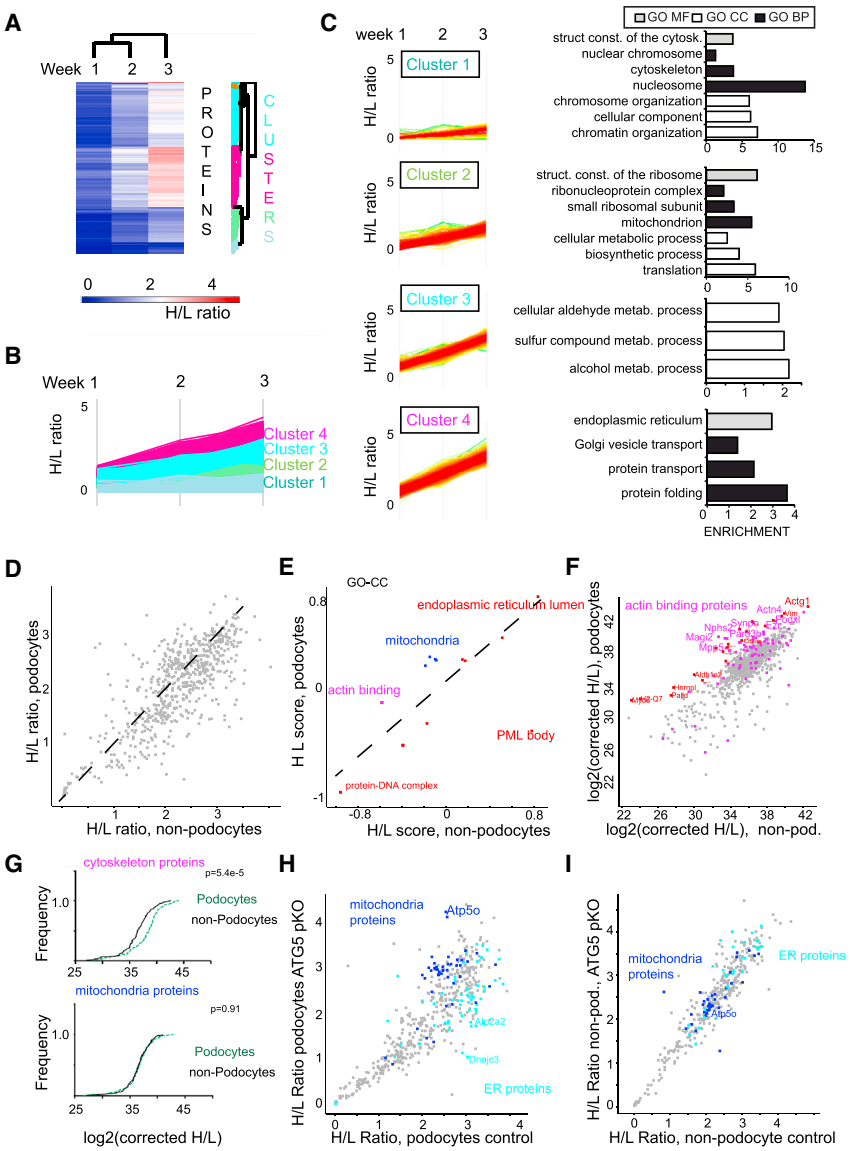

Figure 5. Integration of Podocyte Proteome Dynamics and Deep Proteomics Mapping Demonstrate Proteostatic Podocyte Features

(A) Adult mice were fed a diet in which lysine was substituted with stable isotope-labeled $^{13}C_6$ lysine for the indicated times, resulting in a gradual substitution of the endogenous lysine $^{12}C_6$ lysine (light lysine) with $^{13}C_6$ lysine (heavy lysine). Mean H/L ratios of more than 4 animals are depicted.

(B) Hierarchical clustering (maximum distance) of mean protein H/L ratios was performed, and four major row clusters were defined.

(C) GO enrichment of GOMF (black), GOCC (gray), and GOBP (white) terms (Fishers exact test, corrected FDR < 0.05) in each of the 4 major clusters was performed.

(D) Scatterplot of H/L ratios between podocytes and non-podocyte cells demonstrates that podocytes have a generally slower incorporation of stable isotope-labeled lysine.

(E) 2D GO enrichment analysis of H/L ratios of significantly regulated Uniprot keywords of podocytes and non-podocyte cells (FDR < 0.05).

(F) Scatterplot of corrected H/L ratios between podocytes and non-podocytes.

(G) Cumulative histogram of corrected H/L ratios for cytoskeletal and mitochondrial proteins. When H/L ratios are corrected with absolute protein abundance (Dotproduct, see Experimental Procedures for details), mitochondrial proteins have a similar corrected ratio compared with all other proteins.

(H) H/L ratios in podocytes from control mice plotted against H/L ratios in podocytes in Nphs2.Cre:Atg5 fl/fl (ATG5ko) mice. ATP5o is a subunit of the mitochondrial ATP synthase.

(I) H/L ratios in non-podocytes from control mice plotted against H/L ratios in non-podocytes of (ATG5ko) mice.

independent parallel study (Figures S6B and S6C), confirming that mitochondrial proteins were incorporated relatively faster in podocytes compared with the whole kidney. However, this comparison did not respect overall protein amounts, and protein amounts are significantly different between podocytes and non-podocytes (Figure 3A). Thus, a mere relative incorporation rate is not sufficient to estimate how much "energy" a podocyte spends to maintain the specific protein compared with another cell type; this would crucially depend on the copy numbers and, as an ancillary factor, on the size of the protein. Therefore, we corrected the incorporation rates by total protein abundance and size (Experimental Procedures). The analysis revealed that actin-binding proteins and cytoskeletal proteins incorporated heavy amino acids markedly stronger (Figure 5F). Interestingly, four proteins associated with hereditary podocyte disease were in the upper quartile of most dynamic proteins, among these podocin (Nphs2), Cd2ap (Cd2ap), and actinin-4 (Actn4) (Figures 5F and 5G) and Magi2 (Bierzynska et al., 2016; Figure 5F). The number of amino acids incorporated into mitochondrial proteins was not different in podocytes compared with non-podocytes (Figure 5G), which could be explained by low mitochondrial mass (Figure 3) but high turnover of these organelles (Figure 5B). These data indicate that some of the podocyte's unique proteotypic features are partially compensated by increased protein synthesis and, potentially, proteostasis.

An unexpected finding was that podocytes have high mitochondrial protein synthesis but an overall low protein copy number of mitochondrial proteins. We asked whether this balance would tilt further when genetic manipulation of podocyte proteostasis was performed. We performed quantitative pulse labeling of amino acids in young control mice as well as in young mice with podocyte-specific knockout of autophagy-related 5 (ATG5 podocyte specific knockout [pKO]), a major positive regulator of autophagy in general and especially in podocytes (Hartleben

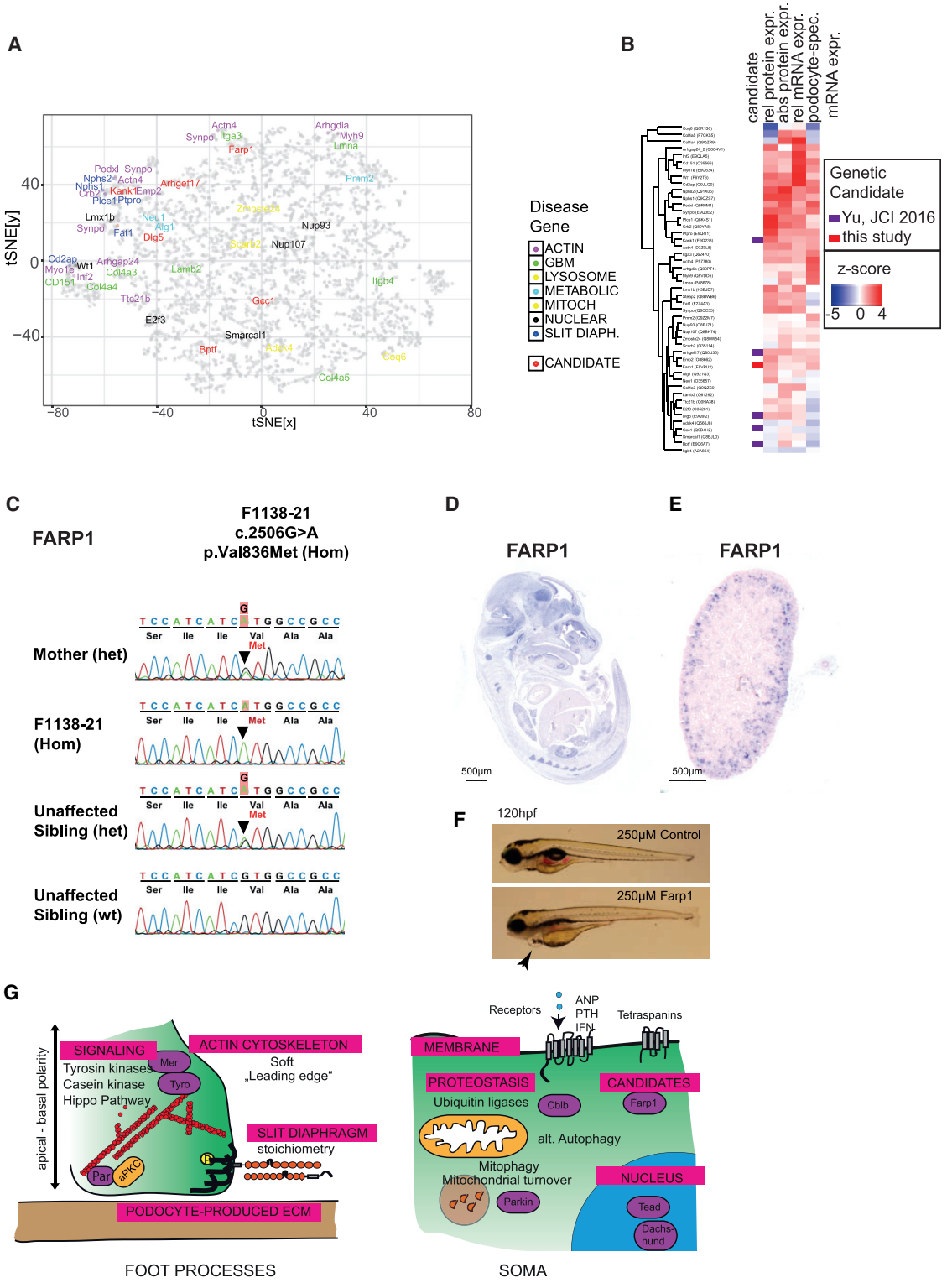

Figure 6. Identification of Candidates for Human Nephrotic Syndrome Disease-Causing Genes

(A) Clustering analysis (t-SNE) of 6,700 proteins for which absolute protein expression, relative protein expression, mRNA expression, and tissue-specific mRNA expression were available.

(B) Heatmap analysis of expression of disease genes and one previously unreported candidate gene, FARP1, as well as five candidates from a previous study (Yu et al., 2016).

(legend continued on next page)

et al., 2010; Table S6). The ATG5 pKO allele makes podocytes extremely susceptible to damage (Hartleben et al., 2010). We observed that ATG5 knockout podocytes had a significantly lower incorporation of endoplasmic reticulum proteins, a finding expected from a defect in autophagy, and, surprisingly a significantly higher incorporation of mitochondrial proteins compared with control podocytes (Figure 5H). This was consistent with 2D GO enrichment time points after different time points (Figures S6D and S6E). Isotope-labeled lysine incorporation in non-podocyte cells was not changed dramatically across both conditions (Figure 5I). In conclusion, these data delineate a specific perturbation in isotope incorporation in podocytes, specifically affecting mitochondria.

Multi-omics Integration Reveals Candidate Genes for Podocyte Function in Humans

Finally, we asked whether the integration of genomic and proteomic analyses could reveal candidate genes essential for podocyte function. To this end, we performed clustering analysis of z-normalized relative mRNA expression levels, relative protein expression levels, absolute protein expression levels, and tissue specificity of podocyte mRNA levels. We found that disease-associated genes in slit diaphragm and actin-related processes were largely defined by very high *Z* scores in all of the four parameters and clustered close to each other (Figures 6A and 6B). Subsequently, we defined 280 genes based on each of these criteria (Table S7) and screened exome sequencing of 430 families with hereditary nephrotic syndrome for homozygous mutations in these genes. As a result, we identified a homozygous mutation in the gene *FARP1* in one family with nephrotic syndrome (Table S7). This candidate gene, and the genes identified in a recent population-based study (Yu et al., 2016), clustered close to known disease genes (Figure 6A), and all shared high *Z* scores in at least three of the four parameters analyzed (Figure 6B). From a genetic perspective, several factors suggest potential pathogenicity of the identified allele: the mutation affects amino acid residues that are highly conserved among orthologs across evolution; in a control database of 80,000 predominantly healthy individuals (Exome Aggregation Consortium [ExAC]), the minor allele frequency of either allele is below 0.01%, and it has not been reported in the homozygous state; and the allele segregates with the affect status within the family (Figure 6C). The mutated residues were highly conserved and the mutation localized in a functional PH domain of the protein, and histology and electron microscopy showed clear signs of podocyte dysfunction within the affected individual (Figures S7A–S7E). A second patient with previously non-identified FARP1 variants was identified in a second cohort of 700 patients with nephrotic syndrome (patient was heterozygous for T789M, and c.-20T > A); however, it was unclear whether the alleles segregated with the phenotype because the DNA of family members could not be sequenced. The FARP1 gene newly identified in this study also localized predominantly to glomeruli and their precursors in development and kidneys of newborn mice (Figures 6D and 6E). In addition, knockdown of the farp1 mRNA in zebrafish larvae resulted in a phenotype of pericardial edema as well as proteinuria, indicating loss of glomerular barrier function in *D. rerio* (Figure 6; Figures S7F and S7G).

DISCUSSION

Postmitotic specialized cell types, such as neurons or podocytes, are particularly vulnerable to age-dependent degeneration. In fact, the podocyte has emerged as a central gatekeeper to prevent proteinuria and renal failure, two unmet and frequent clinical symptoms associated with dramatically increased cardiovascular risk. Interrogation of individual cell types at multiple omics levels can yield insights into both essential molecular components and preventive strategies. Here we gained a near-comprehensive view of the static and dynamic podocyte proteome and transcriptome by applying recently developed technologies (Kulak et al., 2014). Single-cell podocyte sorting previously enabled only incomplete *in vivo* analysis of the podocyte proteome (Boerries et al., 2013; Rinschen et al., 2015a, 2016a). At least 10,000 proteins are suggested to be expressed in a cultured cell line (Kulak et al., 2014; Mann et al., 2013; Nagaraj et al., 2011), and a similar number of proteins has been shown to be expressed in native neurons (Sharma et al., 2015). Here we demonstrate that such a comprehensive atlas of protein and mRNA expression datasets now allows distilling molecular characteristic features of podocytes, ultimately up to the prediction of candidate genes associated with human disease. Figure 6G gives an overview of the findings in this study.

Podocytes express a high abundance of actin-binding proteins and proteins known to be localizing to the leading edge of the cell (Figures 1, 2, and 3; Table S5). Expressed in simplified terms, many of these proteins oppose the formation of stress fibers by promoting actin branching to promote a "motile" phenotype (Higgs and Pollard, 2001). The leading edge is a long-established model to study the cell biology of podocyte foot processes, and eventual slit diaphragm signaling (Garg and Holzman, 2012; Garg et al., 2010; Moeller et al., 2004), and based on these global proteomic data, this paradigm could be further expanded. This study discovered signaling molecules enriched in podocytes, which may be directly translated to novel experimental studies. Several of the proteins, but by far not all of them, have already been studied in podocytes and have been linked in part by dramatic phenotypes in conditional and targeted mouse models (e.g., protein kinase C) (Huber et al., 2009) or human patients (e.g., MAGI2; Bierzynska et al., 2016). A

(C) Sanger sequencing of the respective regions of *FARP1* demonstrates segregation of the mutated alleles with the affected status in family F1138 (*FARP1*).
(D and E) Embryonic and renal expression profile of the candidate protein Farp1 by *in situ* hybridization.
(D) Farp1 shows high expression in metanephric glomerular precursors and readily detectable expression in neuronal tissues and, to some extent, in other pulmonary epithelial structures in embryonic day 14.5 (E14.5) mouse embryos.
(E) Farp1 expression is maintained in murine P1 kidneys in glomeruli.
(F) Knockdown of farp1 in zebrafish induces edema and pericardial effusion (arrow), indicating proteinuria and podocyte dysfunction.
(G) Overview of insights into podocyte biology obtained from this study.

significant fraction of these proteins, however, has not been extensively studied and will require further consideration (Table 1; Table S4); for instance, specific members of the tetraspanin family, which were confirmed in *Drosophila* nephrocyte studies as highly conserved functional regulators of filtering cells (Sachs et al., 2012; Figure 3).

In addition to using these data as a resource, one may also delineate "systems-level" features of molecular podocyte identity. To demonstrate this approach in principle, we delineated differences to the proteome of a commonly used immortalized mouse podocyte cell culture line (Rinschen et al., 2016b). Cultured podocytes are widely used to investigate podocyte damage and serve as a model to study the regulation of the cytoskeleton and many other aspects of podocyte biology (Lee et al., 2015a; Shankland, 2006; Yu et al., 2013). Surprisingly, the systems-level comparison of proteome-wide expression data (Figure 4) revealed that proteins involved in stress fiber formation are among the strongest dysregulated processes in cell cultures, a finding that could be caused by stiffness of the cell culture dish (Gilbert et al., 2010). As a proof-of-principle experiment, the cultivation of either human or mouse podocyte cells on soft matrices resulted in a major shift in the proteome, which partly reduced this actin-related cell culture artefact (Figure 4). This is consistent with observations that podocytes strongly react to other mechanical cues, such as hydrostatic pressure (Kriz and Lemley, 2015), stretch (Durvasula et al., 2004; Kim et al., 2013; Petermann et al., 2005), or membrane curvature (Inoue and Ishibe, 2015), *in vitro* and *in vivo* (Hu et al., 2017; Rinschen et al., 2017). Cultivation on soft matrices does not, however, increase the expression of podocyte-specific actin binders or podocyte membrane proteins, which are only minimally expressed under both conditions.

Mitochondrial proteins are rarely expressed in podocytes (Figure 3), but the synthesis of these proteins (as measured by *in vivo* stable isotope pulse labeling) is faster than in non-podocytes. Therefore, the podocyte has an overall low abundance of mitochondrial proteins but high mitochondrial resynthesis and, assuming a steady-state equilibrium, also turnover. This may be a surrogate readout of predominant mitochondrial degradation (e.g., by mitophagy) in podocytes compared with other glomerular cell types. Consistently, podocytes show protein-level enrichment for the ubiquitin ligase Parkin2 (log2 fold change 2.33), a key molecule controlling mitophagy (Narendra et al., 2008; Table S2). Interestingly, when knocking out ATG5, a protein essential for autophagy (Hartleben et al., 2010), the podocyte reacts, when still intact and functional, with even further increased synthesis of mitochondrial proteins (Figure 5H). One could speculate that this finding may be caused by increased alternative autophagy and mitophagy, a process significantly increased in the absence of ATG5 (Hirota et al., 2015). In fact, mediators of alternative autophagy (e.g., Rab9 and Becn1) are abundantly expressed in podocytes but not significantly enriched (Lee et al., 2015b; Table S2). Although these findings need further corroboration, these data demonstrate the feasibility to dissolve dynamic proteostatic shifts *in vivo* by integrating dynamic and static protein quantifications and cutting through the various dimensions of podocyte proteostasis.

In summary, these data provide a unique resource and starting point for the next level of systematic understanding of podocyte identity, function, and glomerular disease mechanisms, including a systems view of podocyte proteome dynamics (Figure 6G). Using a multidimensional analysis, we showed that a majority of podocyte disease genes (mainly slit diaphragm- and actin-related genes) have rather high relative and absolute protein expression as well as podocyte-specific mRNA expression (Figures 6A and 6B). This opens the door for a potential integrative "reverse genetic" approach to predict functionally relevant candidate genes associated with human podocyte diseases (Figure 6; Table S7) and prioritize them for further functional testing, in particular when more advanced bioinformatics methods are utilized and further data (e.g., transcriptome data from patient cohorts) are integrated. The concept presented here will be advantageous for understanding cell-type-specific function in health and disease.

EXPERIMENTAL PROCEDURES

Animals

$Gt(ROSA)^{26Sortm4(ACTB-tdTomato,-EGFP)Luo/J}$ mice were purchased from The Jackson Laboratory (Bar Harbour, Massachusetts, USA) (Muzumdar et al., 2007), and Tg(NPHS2-cre)295Lbh mice were a generous gift from M. Möller (University of Aachen, Aachen, Germany). Use of $Atg5^{flox}$ mice has been reported previously (Hartleben et al., 2010). In general, $Gt(ROSA)^{26Sortm4(ACTB-tdTomato,-EGFP)Luo/J}$; Tg(NPHS2-cre)295Lbh mice (for deep proteome, RNA-seq, and pulsed *in vivo* stable isotope labeling experiments) as well as $Gt(ROSA)^{26Sortm4(ACTB-tdTomato,-EGFP)Luo/J}$; Tg(NPHS2-cre)295Lbh;$Atg5^{flox/flox}$ mice (pulsed *in vivo* stable isotope labeling experiments) were on a mixed genetic background (Sv129/C57Bl6/ICR). Breeding and genotyping was done according to standard procedures. Mice were housed in an SPF facility with free access to chow and water and a 12-hr day/night cycle. All animal experiments were conducted according to the guidelines of the American Physiological Society as well as the German law for the welfare of animals and were approved by local authorities (Regierungspräsidium Freiburg X12/06J, G11-38, and G11-34). Glomeruli and, subsequently, podocytes were isolated using essential the same method as described previously (Boerries et al., 2013). For details, see Glomerular Isolation and Podocyte Preparation in the Supplemental Experimental Procedures.

Liquid Chromatography-Tandem Mass Spectrometry Acquistion

For details regarding sample preparation of native podocytes for proteomic analysis, see the Supplemental Experimental Procedures. Analysis of peptides was performed using a quadrupole-orbitrap mass spectrometer (Q Exactive Plus, Thermo Scientific, Bremen) coupled to a nano-liquid chromatography (nLC) device. The mass spectrometers were calibrated weekly. Briefly, peptides were separated by nLC using a 4-hr gradient (flow rate, 200 nL/min). Peptides were separated on an in-house packed 50-cm column with 1.7-μm C18 beads (Dr. Maisch). Ascending concentrations of buffer B (80% acetonitrile, 0.1% formic acid) over buffer A (0.1% formic acid) were used. Then peptides were sprayed into the mass spectrometer by electron spray ionization. The acquisition parameters for the mass spectrometer were as described previously (Bartram et al., 2016). 1E6 was the AGC target for MS1. The resolution was 70,000 (mass range, 200–1200 $mz-1$). Tandem mass spectrometry (MS/MS) spectra of the top 10 most intense peaks were obtained by higher-energy collisional dissociation fragmentation. Resolution for the MS/MS spectra was 35,000 at 200 $mz-1$, AGC target to 5E5.

Cell Culture and Proteomics Analysis

Validated cell lines were regularly tested for mycoplasms using a commercial kit (VENOR, Sigma). Human podocytes (Saleem et al., 2002) were cultured in dishes as described previously at 33°C (Rinschen et al., 2016a). They were seeded on collagen-coated soft matrices (Matrigen) for 2 days (passage

~20). Similarly, mouse podocytes (at 33°C) (Griffin et al., 2004) were cultured in coated Primaria cell culture dishes (Falcon) as described previously and seeded on collagen-coated soft matrices (Matrigen) for 2 days. For details regarding sample preparation, proteomics, and bioinformatics analysis, see the Supplemental Experimental Procedures.

Pulsed *In Vivo* Stable Isotope Labeling

Stable isotope labeling of animals was performed as described previously by Krüger et al. (2008). The Lys(0)-stable isotope labeling by amino acid in cell culture (SILAC)-Mouse control ($^{12}C_6$-lysine, "light") and Lys(6)-SILAC-Mouse SILAC ($^{13}C_6$-lysine, 97%, "heavy") mouse diets were purchased from Silantes (Martinsried, Germany). For details regarding sample preparation and proteomics of *in vivo* stable isotope-labeled tissue, see the Supplemental Experimental Procedures.

Statistics

For quantitative data, statistical tests (two tailed unpaired t test, Kolmogorov-Smirnov test, and two-way ANOVA test) were performed where appropriate and where indicated. In general, $p < 0.05$ was considered significant. For large-scale data, correction for multiple testing was performed as described in the respective bioinformatics method sections.

Study Participants, Whole-Exome Sequencing, Multi-gene Panel Testing, and Mutation Calling

We obtained blood samples and pedigrees following informed consent from individuals with steroid resistant nephrotic syndrome (SRNS) or their legal guardians. Approval for human subject research was obtained from the institutional review boards of the University of Michigan and Boston Children's Hospital. For details regarding whole-exome sequencing, multi-gene panel testing, and mutation calling, see the Supplemental Experimental Procedures.

Model Organism Experiments

The detailed methods for functional analysis of zebrafish and *Drosophila* proteinuric phenotypes as well as mouse *in situ* hybridization experiments can be found in the Supplemental Experimental Procedures.

SUPPLEMENTAL INFORMATION

Supplemental Information includes Supplemental Experimental Procedures, seven figures, and seven tables and can be found with this article online at https://doi.org/10.1016/j.celrep.2018.04.059.

ACKNOWLEDGMENTS

We thank Ruth Herzog, Charlotte Meyer, Temel Kilic, Valerie Oberüber, Christine Gretzmeier, and Barbara Joch for expert technical assistance and all members of our laboratories for helpful discussions. This study was supported by the German Research Foundation (DFG) UoC postdoctoral grant and a DFG fellowship (Ri 2811/1-1) (to M.M.R.), CRC 1140 (to F.G., C.B., and T.B.H.), KFO 329 (to T.B. and B.S.) CRC 992 (to T.B.H.), the Heisenberg program (to T.B.H.), and HU 1016/5-1 and HU 1016/8-1 (to T.B.H.); by a European Research Council (ERC) grant (to T.B.H.) and by the H2020-IMI2 Consortium BEAt-DKD (115974 to T.B.H.); by BMBF STOP-FSGS 01GM1518C (to T.B.H.); by the Excellence Initiative of the German Federal and State Governments (BIOSS) (to T.B.H.) and the Freiburg Institute for Advanced Studies (FRIAS) (to T.B.H.); and by the Else Kröner Fresenius Stiftung, NAKSYS (to T.B.H.). C.B. was supported by the Federal Ministry of Education and Research (BMBF, 01GM1515C, Project 2.3). M.B. is funded by BMBF within the framework of the e:Med Research and Funding Concept (DeCaRe, FKZ 01ZX1409B) and by DFG Collaborative Research Center (CRC) 850, Projects Z1 and C9. H.B. acknowledges funding through the DFG Excellence Cluster EXC 306. M.S. was supported by the Fritz Thyssen Foundation (10.16.2.026MN) and BMBF Grant 01GM1518A. F.H. was supported by the NIH (R01-DK076683). M.G. was supported by the German Society of Nephrology (Forschungsstipendium der Deutschen Gesellschaft für Nephrologie 2012). We thank the Yale Center for Mendelian Genomics (U54HG006504) for whole-exome sequencing.

AUTHOR CONTRIBUTIONS

M.M.R., M.G., F.G., T.B., and T.B.H. designed the research studies. M.M.R., M.G., F.G., S.Z., M.H., O.K., M.Z., D.A.B., S.D., C.P., C.T., H.Y.G., and V.K. conducted experiments. G.D., M.P., D.A.B., E. K., C. B., and F.H. acquired genetic data. M.S. and P.S. performed zebrafish experiments. M.M.R., M.G., B.S., M.B., H.B., J.D., and T.B.H. analyzed data. M.K. and J.D. provided reagents and novel tools. M.M.R., M.G., F.G., T.B., and T.B.H. wrote the manuscript.

DECLARATION OF INTERESTS

F.H. is a founder of Goldfinch-Bio and a member of its scientific advisory board. C.B. and E.K. are employees of Bioscientia/Sonic Healthcare. C.B. holds a part-time faculty appointment at the University of Freiburg.

Received: October 18, 2017
Revised: February 7, 2018
Accepted: April 15, 2018
Published: May 22, 2018

REFERENCES

Bartram, M.P., Habbig, S., Pahmeyer, C., Höhne, M., Weber, L.T., Thiele, H., Altmüller, J., Kottoor, N., Wenzel, A., Krueger, M., et al. (2016). Three-layered proteomic characterization of a novel ACTN4 mutation unravels its pathogenic potential in FSGS. Hum. Mol. Genet. *25*, 1152–1164.

Bierzynska, A., Soderquest, K., and Koziell, A. (2015). Genes and podocytes - new insights into mechanisms of podocytopathy. Front. Endocrinol. (Lausanne) *5*, 226.

Bierzynska, A., Soderquest, K., Dean, P., Colby, E., Rollason, R., Jones, C., Inward, C.D., McCarthy, H.J., Simpson, M.A., Lord, G.M., et al. (2016). MAGI2 Mutations Cause Congenital Nephrotic Syndrome. J. Am. Soc. Nephrol. *28*, 1614–1621.

Boerries, M., Grahammer, F., Eiselein, S., Buck, M., Meyer, C., Goedel, M., Bechtel, W., Zschiedrich, S., Pfeifer, D., Laloë, D., et al. (2013). Molecular fingerprinting of the podocyte reveals novel gene and protein regulatory networks. Kidney Int. *83*, 1052–1064.

Boute, N., Gribouval, O., Roselli, S., Benessy, F., Lee, H., Fuchshuber, A., Dahan, K., Gubler, M.C., Niaudet, P., and Antignac, C. (2000). NPHS2, encoding the glomerular protein podocin, is mutated in autosomal recessive steroid-resistant nephrotic syndrome. Nat. Genet. *24*, 349–354.

Brunskill, E.W., Georgas, K., Rumballe, B., Little, M.H., and Potter, S.S. (2011). Defining the molecular character of the developing and adult kidney podocyte. PLoS ONE *6*, e24640.

Cerami, E., Demir, E., Schultz, N., Taylor, B.S., and Sander, C. (2010). Automated network analysis identifies core pathways in glioblastoma. PLoS ONE *5*, e8918.

CDC. Chronic Kidney Disease (CKD) Surveillance Project. https://nccd.cdc.gov/ckd.

Cox, J., and Mann, M. (2012). 1D and 2D annotation enrichment: a statistical method integrating quantitative proteomics with complementary high-throughput data. BMC Bioinformatics *13* (*Suppl 16*), S12.

Durvasula, R.V., Petermann, A.T., Hiromura, K., Blonski, M., Pippin, J., Mundel, P., Pichler, R., Griffin, S., Couser, W.G., and Shankland, S.J. (2004). Activation of a local tissue angiotensin system in podocytes by mechanical strain. Kidney Int. *65*, 30–39.

Endlich, N., and Endlich, K. (2002). cAMP pathway in podocytes. Microsc. Res. Tech. *57*, 228–231.

Fleuren, E.D.G., Hillebrandt-Roeffen, M.H.S., Flucke, U.E., Te Loo, D.M.W.M., Boerman, O.C., van der Graaf, W.T.A., and Versleijen-Jonkers, Y.M.H. (2014). The role of AXL and the in vitro activity of the receptor tyrosine kinase inhibitor BGB324 in Ewing sarcoma. Oncotarget *5*, 12753–12768.

Fu, J., Wei, C., Lee, K., Zhang, W., He, W., Chuang, P., Liu, Z., and He, J.C. (2016). Comparison of Glomerular and Podocyte mRNA Profiles in Streptozotocin-Induced Diabetes. J. Am. Soc. Nephrol. *27*, 1006–1014.

Garg, P., and Holzman, L.B. (2012). Podocytes: gaining a foothold. Exp. Cell Res. *318*, 955–963.

Garg, P., Verma, R., Cook, L., Soofi, A., Venkatareddy, M., George, B., Mizuno, K., Gurniak, C., Witke, W., and Holzman, L.B. (2010). Actin-depolymerizing factor cofilin-1 is necessary in maintaining mature podocyte architecture. J. Biol. Chem. *285*, 22676–22688.

Gilbert, P.M., Havenstrite, K.L., Magnusson, K.E.G., Sacco, A., Leonardi, N.A., Kraft, P., Nguyen, N.K., Thrun, S., Lutolf, M.P., and Blau, H.M. (2010). Substrate elasticity regulates skeletal muscle stem cell self-renewal in culture. Science *329*, 1078–1081.

Grahammer, F., Schell, C., and Huber, T.B. (2013). The podocyte slit diaphragm–from a thin grey line to a complex signalling hub. Nat. Rev. Nephrol. *9*, 587–598.

Griffin, S.V., Hiromura, K., Pippin, J., Petermann, A.T., Blonski, M.J., Krofft, R., Takahashi, S., Kulkarni, A.B., and Shankland, S.J. (2004). Cyclin-dependent kinase 5 is a regulator of podocyte differentiation, proliferation, and morphology. Am. J. Pathol. *165*, 1175–1185.

Gurkan, S., Cabinian, A., Lopez, V., Bhaumik, M., Chang, J.-M., Rabson, A.B., and Mundel, P. (2013). Inhibition of type I interferon signalling prevents TLR ligand-mediated proteinuria. J. Pathol. *231*, 248–256.

Harita, Y., Kurihara, H., Kosako, H., Tezuka, T., Sekine, T., Igarashi, T., and Hattori, S. (2008). Neph1, a component of the kidney slit diaphragm, is tyrosine-phosphorylated by the Src family tyrosine kinase and modulates intracellular signaling by binding to Grb2. J. Biol. Chem. *283*, 9177–9186.

Hartleben, B., Gödel, M., Meyer-Schwesinger, C., Liu, S., Ulrich, T., Köbler, S., Wiech, T., Grahammer, F., Arnold, S.J., Lindenmeyer, M.T., et al. (2010). Autophagy influences glomerular disease susceptibility and maintains podocyte homeostasis in aging mice. J. Clin. Invest. *120*, 1084–1096.

Higgs, H.N., and Pollard, T.D. (2001). Regulation of actin filament network formation through ARP2/3 complex: activation by a diverse array of proteins. Annu. Rev. Biochem. *70*, 649–676.

Hirota, Y., Yamashita, S., Kurihara, Y., Jin, X., Aihara, M., Saigusa, T., Kang, D., and Kanki, T. (2015). Mitophagy is primarily due to alternative autophagy and requires the MAPK1 and MAPK14 signaling pathways. Autophagy *11*, 332–343.

Hodgin, J.B., Nair, V., Zhang, H., Randolph, A., Harris, R.C., Nelson, R.G., Weil, E.J., Cavalcoli, J.D., Patel, J.M., Brosius, F.C., 3rd, and Kretzler, M. (2013). Identification of cross-species shared transcriptional networks of diabetic nephropathy in human and mouse glomeruli. Diabetes *62*, 299–308.

Hu, M., Azeloglu, E.U., Ron, A., Tran-Ba, K.-H., Calizo, R.C., Tavassoly, I., Bhattacharya, S., Jayaraman, G., Chen, Y., Rabinovich, V., et al. (2017). A biomimetic gelatin-based platform elicits a pro-differentiation effect on podocytes through mechanotransduction. Sci. Rep. *7*, 43934.

Huber, T.B., Hartleben, B., Winkelmann, K., Schneider, L., Becker, J.U., Leitges, M., Walz, G., Haller, H., and Schiffer, M. (2009). Loss of podocyte aPKClambda/iota causes polarity defects and nephrotic syndrome. J. Am. Soc. Nephrol. *20*, 798–806.

Inoue, K., and Ishibe, S. (2015). Podocyte endocytosis in the regulation of the glomerular filtration barrier. Am. J. Physiol. Renal Physiol. *309*, F398–F405.

Janmey, P.A., and Miller, R.T. (2011). Mechanisms of mechanical signaling in development and disease. J. Cell Sci. *124*, 9–18.

Ju, W., Smith, S., and Kretzler, M. (2012). Genomic biomarkers for chronic kidney disease. Transl. Res. *159*, 290–302.

Kann, M., Ettou, S., Jung, Y.L., Lenz, M.O., Taglienti, M.E., Park, P.J., Schermer, B., Benzing, T., and Kreidberg, J.A. (2015). Genome-Wide Analysis of Wilms' Tumor 1-Controlled Gene Expression in Podocytes Reveals Key Regulatory Mechanisms. J. Am. Soc. Nephrol. *26*, 2097–2104.

Kaplan, J.M., Kim, S.H., North, K.N., Rennke, H., Correia, L.A., Tong, H.Q., Mathis, B.J., Rodríguez-Pérez, J.C., Allen, P.G., Beggs, A.H., and Pollak, M.R. (2000). Mutations in ACTN4, encoding alpha-actinin-4, cause familial focal segmental glomerulosclerosis. Nat. Genet. *24*, 251–256.

Kestilä, M., Lenkkeri, U., Männikkö, M., Lamerdin, J., McCready, P., Putaala, H., Ruotsalainen, V., Morita, T., Nissinen, M., Herva, R., et al. (1998). Positionally cloned gene for a novel glomerular protein–nephrin–is mutated in congenital nephrotic syndrome. Mol. Cell *1*, 575–582.

Kim, E.Y., Anderson, M., Wilson, C., Hagmann, H., Benzing, T., and Dryer, S.E. (2013). NOX2 interacts with podocyte TRPC6 channels and contributes to their activation by diacylglycerol: essential role of podocin in formation of this complex. Am. J. Physiol. Cell Physiol. *305*, C960–C971.

Kim, M.-S., Pinto, S.M., Getnet, D., Nirujogi, R.S., Manda, S.S., Chaerkady, R., Madugundu, A.K., Kelkar, D.S., Isserlin, R., Jain, S., et al. (2014). A draft map of the human proteome. Nature *509*, 575–581.

Kohli, P., Bartram, M.P., Habbig, S., Pahmeyer, C., Lamkemeyer, T., Benzing, T., Schermer, B., and Rinschen, M.M. (2014). Label-free quantitative proteomic analysis of the YAP/TAZ interactome. Am. J. Physiol. Cell Physiol. *306*, C805–C818.

Köttgen, A., Pattaro, C., Böger, C.A., Fuchsberger, C., Olden, M., Glazer, N.L., Parsa, A., Gao, X., Yang, Q., Smith, A.V., et al. (2010). New loci associated with kidney function and chronic kidney disease. Nat. Genet *42*, 376–384.

Kriz, W., and Lemley, K.V. (2015). A potential role for mechanical forces in the detachment of podocytes and the progression of CKD. J. Am. Soc. Nephrol. *26*, 258–269.

Krüger, M., Moser, M., Ussar, S., Thievessen, I., Luber, C.A., Forner, F., Schmidt, S., Zanivan, S., Fässler, R., and Mann, M. (2008). SILAC mouse for quantitative proteomics uncovers kindlin-3 as an essential factor for red blood cell function. Cell *134*, 353–364.

Kulak, N.A., Pichler, G., Paron, I., Nagaraj, N., and Mann, M. (2014). Minimal, encapsulated proteomic-sample processing applied to copy-number estimation in eukaryotic cells. Nat. Methods *11*, 319–324.

Lee, H.W., Khan, S.Q., Faridi, M.H., Wei, C., Tardi, N.J., Altintas, M.M., Elshabrawy, H.A., Mangos, S., Quick, K.L., Sever, S., et al. (2015a). A Podocyte-Based Automated Screening Assay Identifies Protective Small Molecules. J. Am. Soc. Nephrol. *26*, 2741–2752.

Lee, J.W., Chou, C.-L., and Knepper, M.A. (2015b). Deep Sequencing in Microdissected Renal Tubules Identifies Nephron Segment-Specific Transcriptomes. J. Am. Soc. Nephrol. *26*, 2669–2677.

Lee-Sherick, A.B., Zhang, W., Menachof, K.K., Hill, A.A., Rinella, S., Kirkpatrick, G., Page, L.S., Stashko, M.A., Jordan, C.T., Wei, Q., et al. (2015). Efficacy of a Mer and Flt3 tyrosine kinase small molecule inhibitor, UNC1666, in acute myeloid leukemia. Oncotarget *6*, 6722–6736.

Liu, Y., Beyer, A., and Aebersold, R. (2016). On the Dependency of Cellular Protein Levels on mRNA Abundance. Cell *165*, 535–550.

Mann, M., Kulak, N.A., Nagaraj, N., and Cox, J. (2013). The coming age of complete, accurate, and ubiquitous proteomes. Mol. Cell *49*, 583–590.

Meguid El Nahas, A., and Bello, A.K. (2005). Chronic kidney disease: the global challenge. Lancet *365*, 331–340.

Moeller, M.J., Soofi, A., Braun, G.S., Li, X., Watzl, C., Kriz, W., and Holzman, L.B. (2004). Protocadherin FAT1 binds Ena/VASP proteins and is necessary for actin dynamics and cell polarization. EMBO J. *23*, 3769–3779.

Muzumdar, M.D., Tasic, B., Miyamichi, K., Li, L., and Luo, L. (2007). A global double-fluorescent Cre reporter mouse. Genesis *45*, 593–605.

Nagaraj, N., Wisniewski, J.R., Geiger, T., Cox, J., Kircher, M., Kelso, J., Pääbo, S., and Mann, M. (2011). Deep proteome and transcriptome mapping of a human cancer cell line. Mol. Syst. Biol. *7*, 548.

Narendra, D., Tanaka, A., Suen, D.-F., and Youle, R.J. (2008). Parkin is recruited selectively to impaired mitochondria and promotes their autophagy. J. Cell Biol. *183*, 795–803.

New, L.A., Martin, C.E., and Jones, N. (2014). Advances in slit diaphragm signaling. Curr. Opin. Nephrol. Hypertens. *23*, 420–430.

Pavenstädt, H., Kriz, W., and Kretzler, M. (2003). Cell biology of the glomerular podocyte. Physiol. Rev. *83*, 253–307.

Petermann, A.T., Pippin, J., Durvasula, R., Pichler, R., Hiromura, K., Monkawa, T., Couser, W.G., and Shankland, S.J. (2005). Mechanical stretch induces podocyte hypertrophy in vitro. Kidney Int. *67*, 157–166.

Reiser, J., Polu, K.R., Möller, C.C., Kenlan, P., Altintas, M.M., Wei, C., Faul, C., Herbert, S., Villegas, I., Avila-Casado, C., et al. (2005). TRPC6 is a glomerular slit diaphragm-associated channel required for normal renal function. Nat. Genet. *37*, 739–744.

Rinschen, M.M., Wu, X., König, T., Pisitkun, T., Hagmann, H., Pahmeyer, C., Lamkemeyer, T., Kohli, P., Schnell, N., Schermer, B., et al. (2014). Phosphoproteomic Analysis Reveals Regulatory Mechanisms at the Kidney Filtration Barrier. J. Am. Soc. Nephrol. *25*, 1509–1522.

Rinschen, M.M., Benzing, T., Limbutara, K., and Pisitkun, T. (2015a). Proteomic analysis of the kidney filtration barrier–Problems and perspectives. Proteomics Clin. Appl. *9*, 1053–1068.

Rinschen, M.M., Pahmeyer, C., Pisitkun, T., Schnell, N., Wu, X., Maaß, M., Bartram, M.P., Lamkemeyer, T., Schermer, B., Benzing, T., et al. (2015b). Comparative phosphoproteomic analysis of mammalian glomeruli reveals conserved podocin C-terminal phosphorylation as a determinant of slit diaphragm complex architecture. Proteomics *15*, 1326–1331.

Rinschen, M.M., Bharill, P., Wu, X., Kohli, P., Reinert, M.J., Kretz, O., Saez, I., Schermer, B., Höhne, M., Bartram, M.P., et al. (2016a). The ubiquitin ligase Ubr4 controls stability of podocin/MEC-2 supercomplexes. Hum. Mol. Genet. *25*, 1328–1344.

Rinschen, M.M., Schroeter, C.B., Koehler, S., Ising, C., Schermer, B., Kann, M., Benzing, T., and Brinkkoetter, P.T. (2016b). Quantitative deep-mapping of the cultured podocyte proteome uncovers shifts in proteostatic mechanisms during differentiation. Am. J. Physiol. Cell Physiol. *311*, C404–C417.

Rinschen, M.M., Grahammer, F., Hoppe, A.-K., Kohli, P., Hagmann, H., Kretz, O., Bertsch, S., Höhne, M., Göbel, H., Bartram, M.P., et al. (2017). YAP-mediated mechanotransduction determines the podocyte's response to damage. Sci. Signal. *10*, eaaf8165.

Sachs, N., Claessen, N., Aten, J., Kreft, M., Teske, G.J.D., Koeman, A., Zuurbier, C.J., Janssen, H., and Sonnenberg, A. (2012). Blood pressure influences end-stage renal disease of Cd151 knockout mice. J. Clin. Invest. *122*, 348–358.

Sadowski, C.E., Lovric, S., Ashraf, S., Pabst, W.L., Gee, H.Y., Kohl, S., Engelmann, S., Vega-Warner, V., Fang, H., Halbritter, J., et al.; SRNS Study Group (2015). A single-gene cause in 29.5% of cases of steroid-resistant nephrotic syndrome. J. Am. Soc. Nephrol. *26*, 1279–1289.

Saleem, M.A., O'Hare, M.J., Reiser, J., Coward, R.J., Inward, C.D., Farren, T., Xing, C.Y., Ni, L., Mathieson, P.W., and Mundel, P. (2002). A conditionally immortalized human podocyte cell line demonstrating nephrin and podocin expression. J. Am. Soc. Nephrol. *13*, 630–638.

Sampson, M.G., Hodgin, J.B., and Kretzler, M. (2015). Defining nephrotic syndrome from an integrative genomics perspective. Pediatr. Nephrol. Berl. Ger. *30*, 51–63, quiz 59.

Savas, J.N., Toyama, B.H., Xu, T., Yates, J.R., 3rd, and Hetzer, M.W. (2012). Extremely long-lived nuclear pore proteins in the rat brain. Science *335*, 942.

Schmieder, S., Nagai, M., Orlando, R.A., Takeda, T., and Farquhar, M.G. (2004). Podocalyxin activates RhoA and induces actin reorganization through NHERF1 and Ezrin in MDCK cells. J. Am. Soc. Nephrol. *15*, 2289–2298.

Schwanhäusser, B., Busse, D., Li, N., Dittmar, G., Schuchhardt, J., Wolf, J., Chen, W., and Selbach, M. (2011). Global quantification of mammalian gene expression control. Nature *473*, 337–342.

Schwartzman, M., Reginensi, A., Wong, J.S., Basgen, J.M., Meliambro, K., Nicholas, S.B., D'Agati, V., McNeill, H., and Campbell, K.N. (2015). Podocyte-Specific Deletion of Yes-Associated Protein Causes FSGS and Progressive Renal Failure. J. Am. Soc. Nephrol. *27*, 216–226.

Shalom, O., Shalva, N., Altschuler, Y., and Motro, B. (2008). The mammalian Nek1 kinase is involved in primary cilium formation. FEBS Lett. *582*, 1465–1470.

Shankland, S.J. (2006). The podocyte's response to injury: role in proteinuria and glomerulosclerosis. Kidney Int. *69*, 2131–2147.

Sharma, K., Schmitt, S., Bergner, C.G., Tyanova, S., Kannaiyan, N., Manrique-Hoyos, N., Kongi, K., Cantuti, L., Hanisch, U.-K., Philips, M.-A., et al. (2015). Cell type- and brain region-resolved mouse brain proteome. Nat. Neurosci. *18*, 1819–1831.

Staffel, J., Valletta, D., Federlein, A., Ehm, K., Volkmann, R., Füchsl, A.M., Witzgall, R., Kuhn, M., and Schweda, F. (2016). Natriuretic Peptide Receptor Guanylyl Cyclase-A in Podocytes is Renoprotective but Dispensable for Physiologic Renal Function. J. Am. Soc. Nephrol. *28*, 260–277.

Susztak, K. (2014). Understanding the epigenetic syntax for the genetic alphabet in the kidney. J. Am. Soc. Nephrol. *25*, 10–17.

Tong, J., Taylor, P., and Moran, M.F. (2014). Proteomic analysis of the epidermal growth factor receptor (EGFR) interactome and post-translational modifications associated with receptor endocytosis in response to EGF and stress. Mol. Cell. Proteomics MCP *13*, 1644–1658.

Toyama, B.H., Savas, J.N., Park, S.K., Harris, M.S., Ingolia, N.T., Yates, J.R., 3rd, and Hetzer, M.W. (2013). Identification of long-lived proteins reveals exceptional stability of essential cellular structures. Cell *154*, 971–982.

Uhlén, M., Fagerberg, L., Hallström, B.M., Lindskog, C., Oksvold, P., Mardinoglu, A., Sivertsson, Å., Kampf, C., Sjöstedt, E., Asplund, A., et al. (2015). Proteomics. Tissue-based map of the human proteome. Science *347*, 1260419.

Vogel, C., and Marcotte, E.M. (2012). Insights into the regulation of protein abundance from proteomic and transcriptomic analyses. Nat. Rev. Genet. *13*, 227–232.

Weavers, H., Prieto-Sánchez, S., Grawe, F., Garcia-López, A., Artero, R., Wilsch-Bräuninger, M., Ruiz-Gómez, M., Skaer, H., and Denholm, B. (2009). The insect nephrocyte is a podocyte-like cell with a filtration slit diaphragm. Nature *457*, 322–326.

Wilhelm, M., Schlegl, J., Hahne, H., Gholami, A.M., Lieberenz, M., Savitski, M.M., Ziegler, E., Butzmann, L., Gessulat, S., Marx, H., et al. (2014). Mass-spectrometry-based draft of the human proteome. Nature *509*, 582–587.

Wirnsberger, G., Zwolanek, F., Asaoka, T., Kozieradzki, I., Tortola, L., Wimmer, R.A., Kavirayani, A., Fresser, F., Baier, G., Langdon, W.Y., et al. (2016). Inhibition of CBLB protects from lethal Candida albicans sepsis. Nat. Med. *22*, 915–923.

Wiśniewski, J.R., Hein, M.Y., Cox, J., and Mann, M. (2014). A "proteomic ruler" for protein copy number and concentration estimation without spike-in standards. Mol. Cell. Proteomics *13*, 3497–3506.

Yu, C.-C., Fornoni, A., Weins, A., Hakroush, S., Maiguel, D., Sageshima, J., Chen, L., Ciancio, G., Faridi, M.H., Behr, D., et al. (2013). Abatacept in B7-1-positive proteinuric kidney disease. N. Engl. J. Med. *369*, 2416–2423.

Yu, H., Artomov, M., Brähler, S., Stander, M.C., Shamsan, G., Sampson, M.G., White, J.M., Kretzler, M., Miner, J.H., Jain, S., et al. (2016). A role for genetic susceptibility in sporadic focal segmental glomerulosclerosis. J. Clin. Invest. *126*, 1067–1078.

Zhang, F., Zhao, Y., and Han, Z. (2013). An in vivo functional analysis system for renal gene discovery in Drosophila pericardial nephrocytes. J. Am. Soc. Nephrol. *24*, 191–197.

Zhang, W., DeRyckere, D., Hunter, D., Liu, J., Stashko, M.A., Minson, K.A., Cummings, C.T., Lee, M., Glaros, T.G., Newton, D.L., et al. (2014). UNC2025, a potent and orally bioavailable MER/FLT3 dual inhibitor. J. Med. Chem. *57*, 7031–7041.

Cell Reports, Volume *23*

Supplemental Information

A Multi-layered Quantitative *In Vivo* Expression Atlas of the Podocyte Unravels Kidney Disease Candidate Genes

Markus M. Rinschen, Markus Gödel, Florian Grahammer, Stefan Zschiedrich, Martin Helmstädter, Oliver Kretz, Mostafa Zarei, Daniela A. Braun, Sebastian Dittrich, Caroline Pahmeyer, Patricia Schroder, Carolin Teetzen, HeonYung Gee, Ghaleb Daouk, Martin Pohl, Elisa Kuhn, Bernhard Schermer, Victoria Küttner, Melanie Boerries, Hauke Busch, Mario Schiffer, Carsten Bergmann, Marcus Krüger, Friedhelm Hildebrandt, Joern Dengjel, Thomas Benzing, and Tobias B. Huber

A

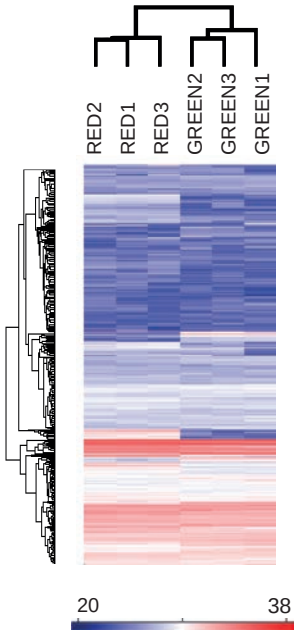
RED2
RED1
RED3
GREEN2
GREEN3
GREEN1
20
38

B

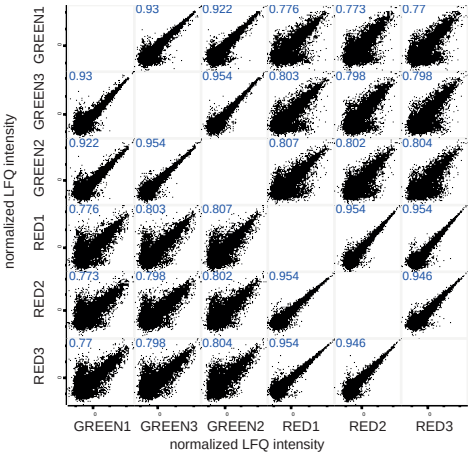
GREEN1
GREEN3
GREEN2
RED1
RED2
RED3
0.93
0.922
0.776
0.773
0.77
0.954
0.803
0.798
0.807
0.802
0.804
0.954
0.946
normalized LFQ intensity
normalized LFQ intensity

C

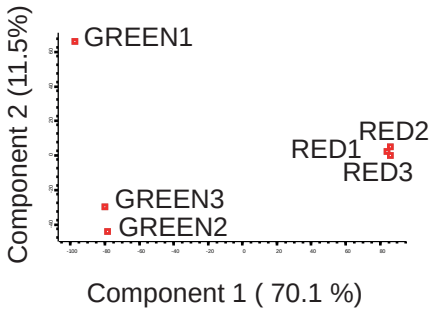
GREEN1
RED2
RED1
RED3
GREEN3
GREEN2
Component 2 (11.5%)
Component 1 (70.1 %)

Fig. S1

Fig. S1. Quality controls of the proteomic dataset, Related to Fig. 1. A. Analysis of lable-free quantitative intensities reveals a strong separation between podocytes (green) and non-podocytes (red) quantitative proteome profiles. B. Multi scatter plots of LFQ intensities indicate a clear separation between podocytes (green) and non-podocytes (red) and a high correlation between biological replicates. Pearson's correlation coefficients are annotated. C. Principal component analysis of protein expression values of samples in this study.

A

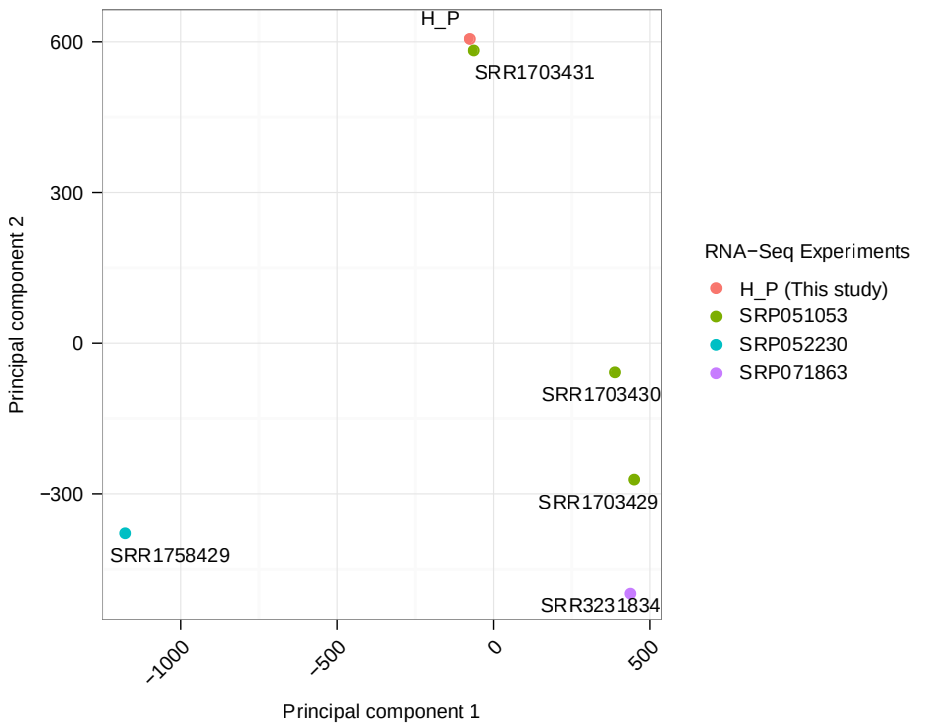

B

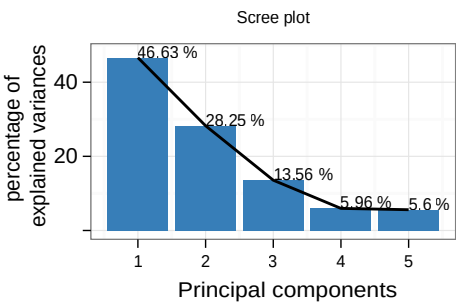

C

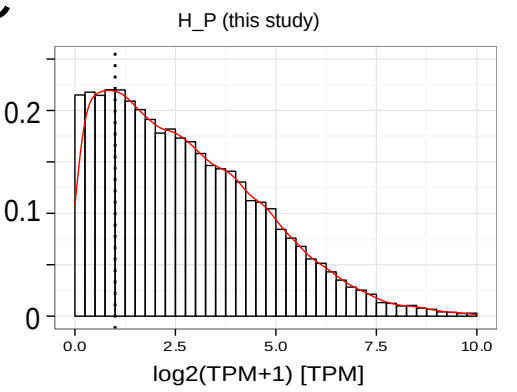

D

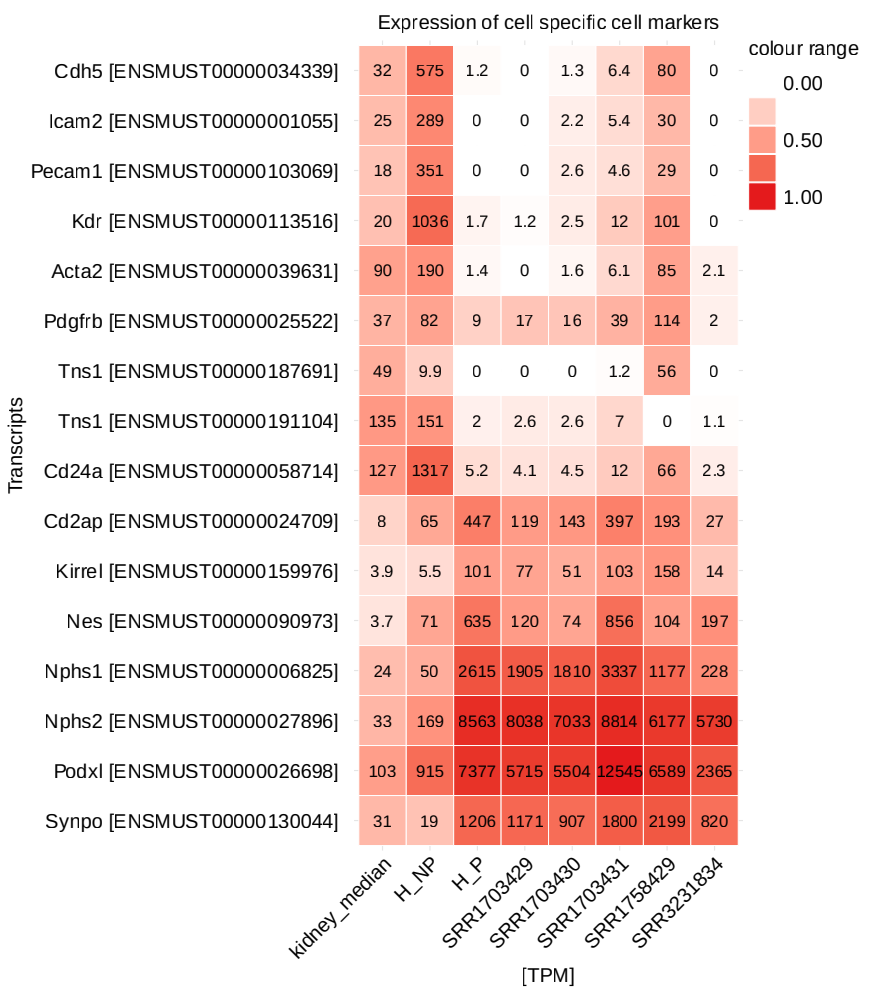

E

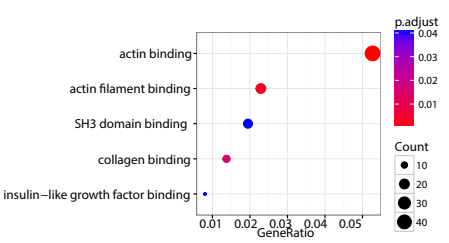

F

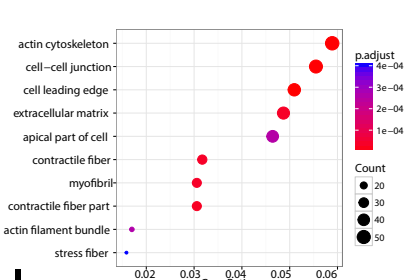

G

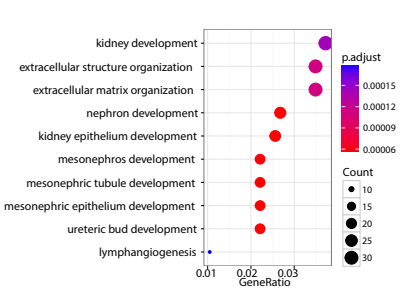

H

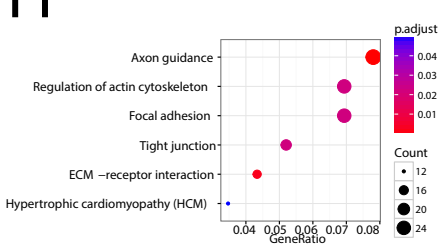

I

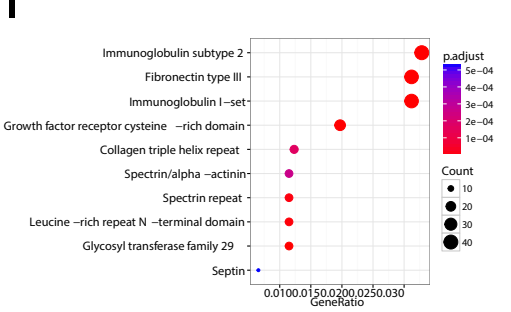

Fig. S2

Fig. S2. Transcriptome quality controls and overexpressed gene sets, Related to Fig. 2. A. PCA analysis of published podocyte mRNA-Seq studies (see Table S3 for details, H_P is our study). B. Contribution to principal components. C. Histogramm and density plot of tpm values from our podocyte mRNA-Seq study. D. Comparison of tpm values of podocyte, mesangial cell and endothelial cell marker genes. Our Podocyte RNA-Seq study as well as the studies of Kann et al.(6) and Fu et al. (8) proofed to be podocyte specific with only minimal expression of mesangial and endothelial marker genes (H_NP is our RNA-Seq study on non-podocyte glomerular cells, H_P is our study on podocytes, see Table S3 for details of further studies). E-I. Overrepresented Genesets in podocyte compared to non-podocyte glomerular cells transcriptomes. Related to Fig. 2. E. GO molecular function. F. GO cellular component. G. GO biological process. H. KEGG-pathway. I. Interpro domains

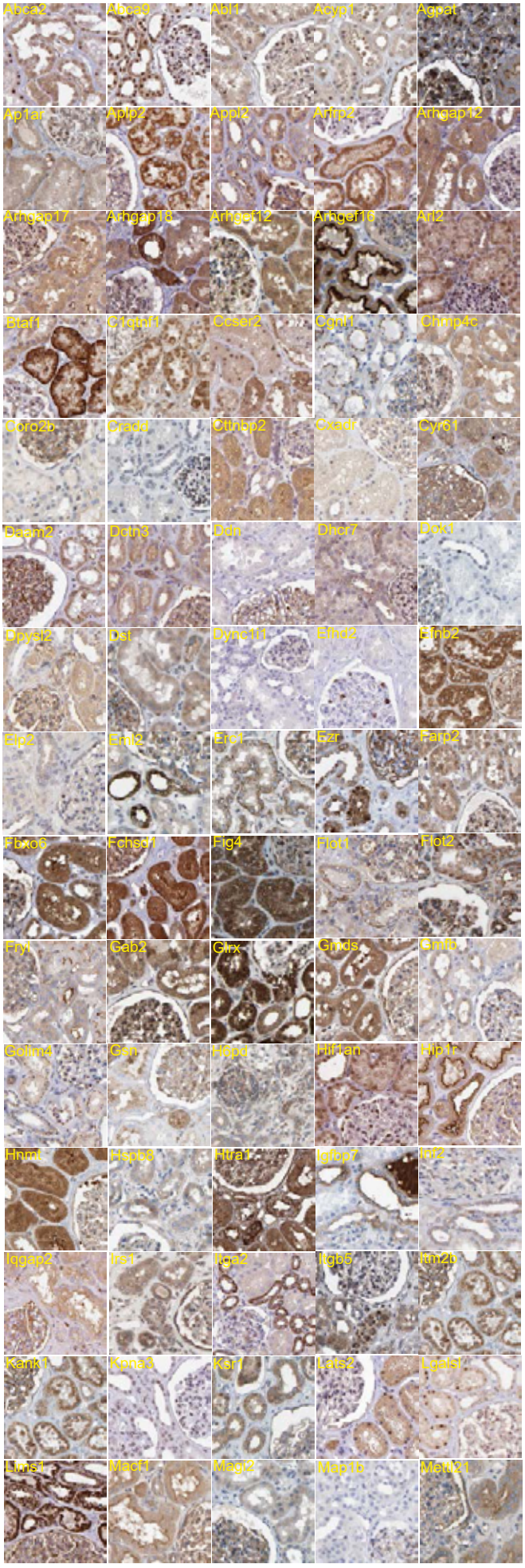
Abca2
Abca3
Abl1
Acyp1
Agpat
Ap1ar
Appl2
Appl2
Arhgap2
Arhgap12
Arhgap17
Arhgap18
Arhgef12
Arhgef18
Arl2
Btaf1
C1qbp1
Ccser2
Cgnl1
Chmp4c
Coro2b
Cradd
Cttnbp2
Cxadr
Cyr61
Daam2
Dctn3
Dlm
Dhcr7
Dok1
Dpysl2
Dst
Dync1i1
Ehd2
Enb2
Epb2
Eml2
Erc1
Ezr
Farp2
Fbxo6
Fchsd1
Fig4
Flot1
Flot2
Fnl
Gab2
Glrx
Gmds
Gnb1
Golm1
Gsn
Hspa8
Hif1an
Hlb1c
Hnrnl
Hspb8
Itga1
Igfbp7
Irf2
Iqgap2
Irs1
Itga2
Itgb5
Itm2b
Kank1
Kcna3
Kdr
Lats2
Lgals1
Lmo1
Mad1l1
Magi2
Map1b
Mcm21

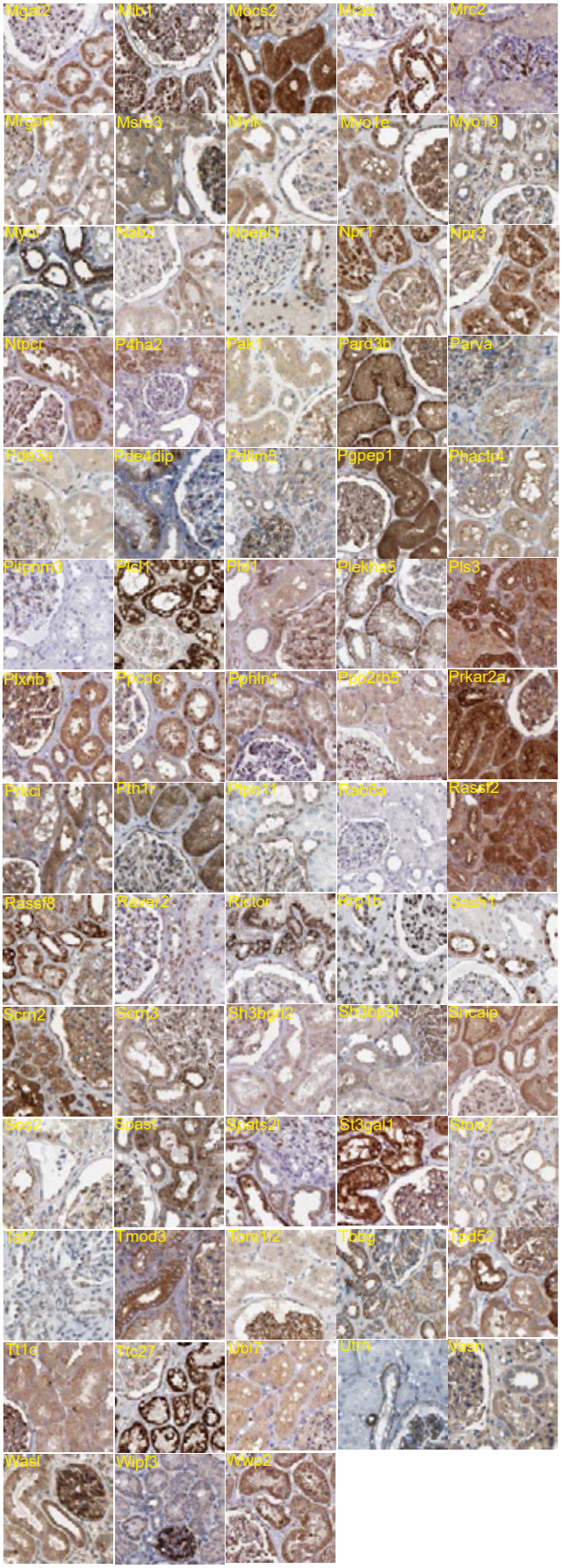
Mgat2
Mib1
Mocs2
Mras
Mrc2
Mrgpr1
Msrb3
Mylk
Myo1e
Myo10
Myof
Nab2
Ndpp1
Npc1
Npc3
Nt5c
P4ha2
Pak1
Pard3b
Parva
Pde3a
Pde4dip
Pdlim5
Pgpep1
Phactr4
Ptprm3
Ptk1
Ptd1
Plekha5
Pls3
Plxnb1
Ppcdc
Pphln1
Ppp2r5
Prkar2a
Prkci
Pth1r
Ptpn11
Ptpcba
Rassf2
Rassf8
Rever2
Rictor
Rnf15
Sash1
Scrn2
Sort1
Sh3bgrl2
Sh3bp5l
Shcalp
Sos2
Spast
Spats2l
St3gal1
Ston2
Tal7
Tmod3
Tom1l2
Tpbg
Tpd52
Tt1c
Ttc27
Ubl7
Utrn
Vasn
Wasl
Wipf3
Wwp2

Fig. S3

Fig. S3: Glomerular staining of podocyte-enriched proteins in the human protein atlas. Related to Fig. 3. Proteins significantly enriched in podocytes were mapped on the human protein atlas (https://www.proteinatlas.org/). The figure shows proteins with “medium” protein staining in the resource. Corresponding mouse gene symbols are annotated.

A

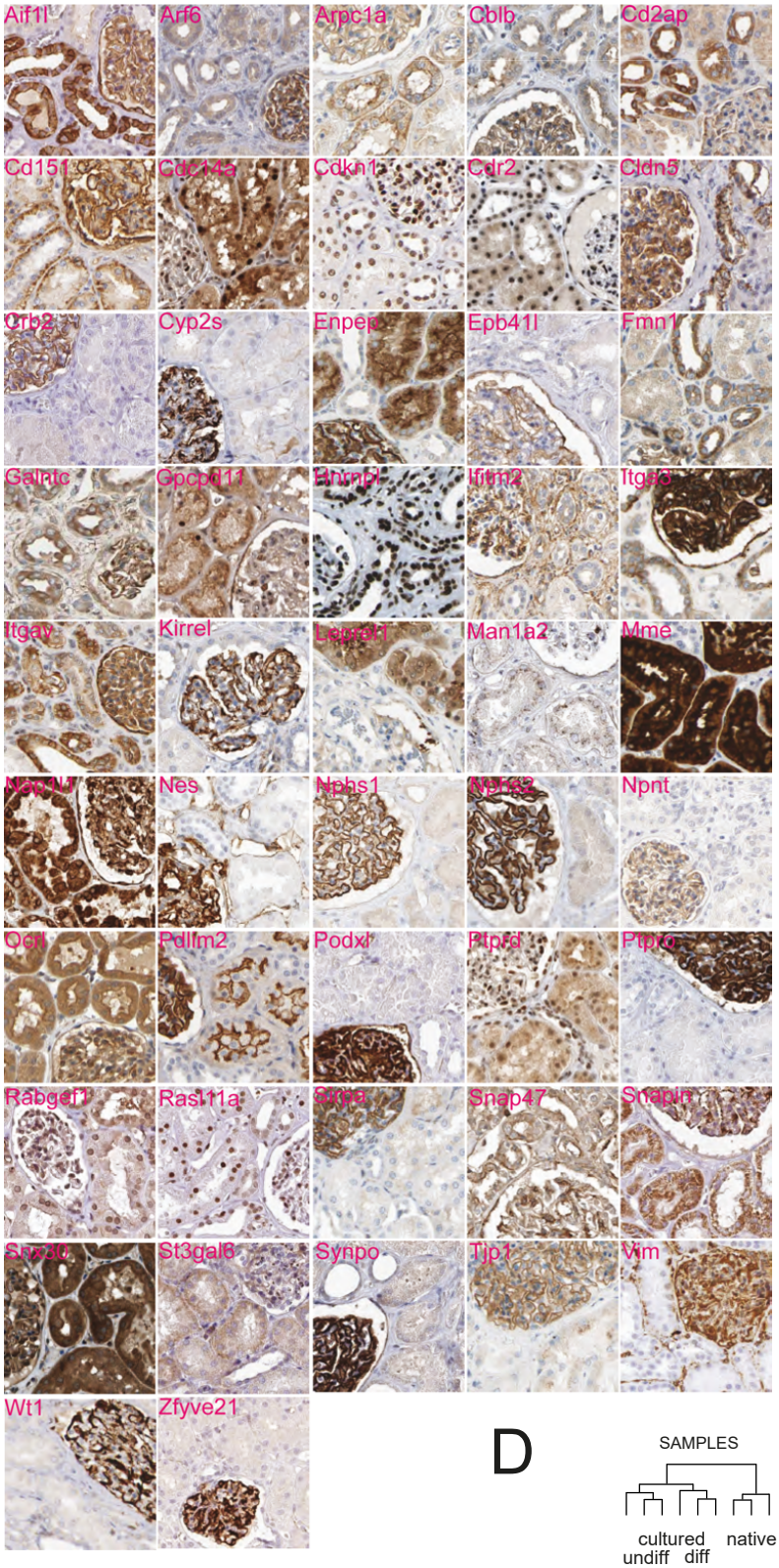
Aif1l
Arf6
Arpc1a
Cblb
Cd2ap
Cd151
Cdc42a
Cdkn1c
Cdr2
Cldn5
Crb2
Cyp2s
Enpep
Epb41l
Fmn1
Galntc
Gpcpd1
Hnrnpl
Ifitm2
Itga3
Itgav
Kirrel
Lasp1
Man1a2
Mme
Nap1l
Nes
Nphs1
Nphs2
Npnt
Qdpr
Pdlim2
Podxl
Ptpro
Ptprq
Rabgef1
Ras11a
Stbd1
Snap47
Snapin
Snx30
St3gal6
Synpo
Tjp1
Vim
Wt1
Zfyve21

B

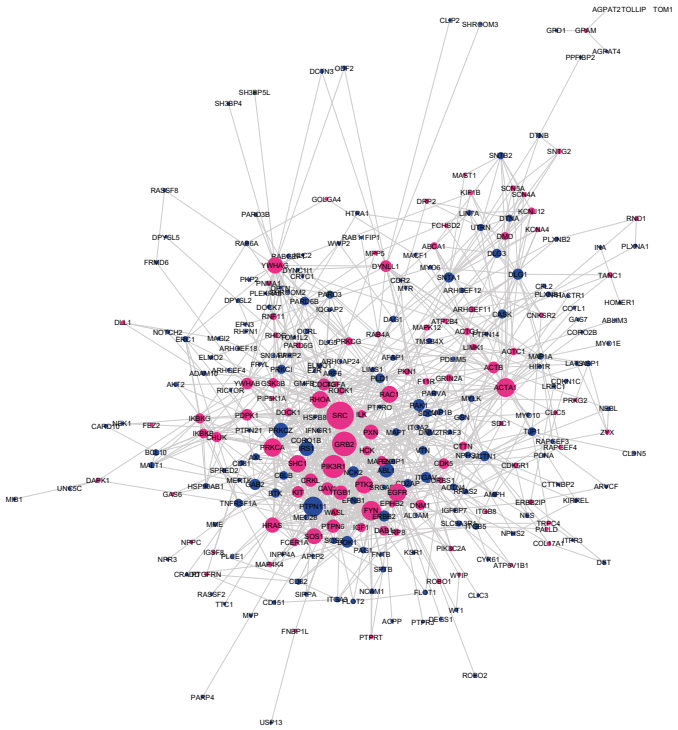

C

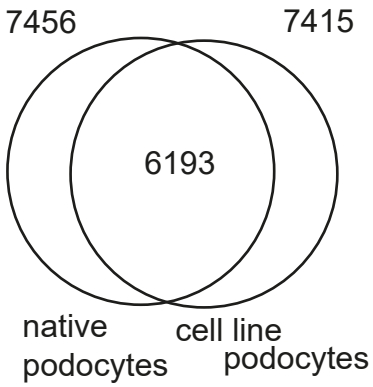
7456
7415
6193
native podocytes
cell line podocytes

D

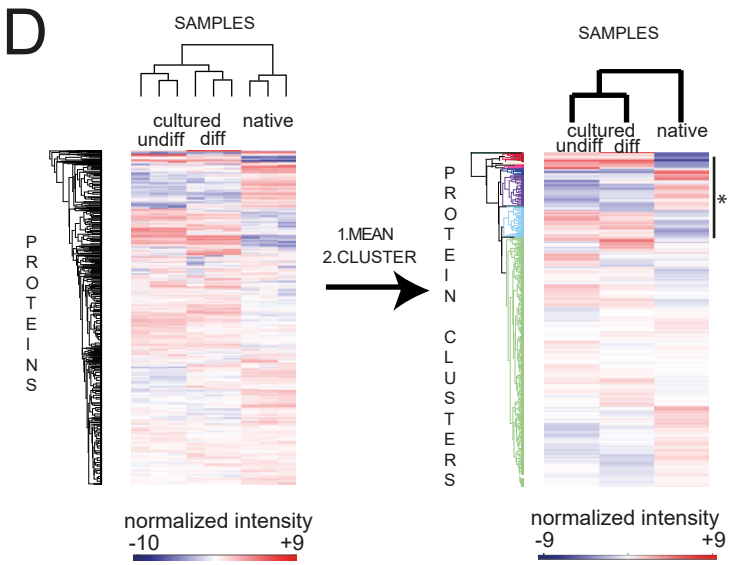
SAMPLES
cultured undiff
diff
native
PROTEINS
normalized intensity
-10
+9
1.MEAN
2.CLUSTER
SAMPLES
cultured undiff
diff
native
PROTEIN CLUSTERS
*
normalized intensity
-9
+9

Fig. S4

Fig. S4. Glomerular staining of podocyte-enriched proteins in the human protein atlas, podocyte-specific interaction network and comparison between cultured and native podocytes, Related to Fig. 3 and 4. A: Proteins significantly enriched in podocytes were mapped on the human protein atlas (https://www.proteinatlas.org/). The figure shows proteins with “strong” protein staining in the resource. Gene symbols are annotated. B. Podocyte-enriched interaction network. Podocyte-enriched proteins (n=541) were analyzed with the Netbox software for common interactors (p-value threshold $p<0.05$). Nodes represent proteins, whereas edges represent interactions. Proteins in the initial dataset of podocyte-specific proteins are depicted in blue, whereas proteins determined as “linker” proteins (not in the initial datasets) are depicted in magenta. The node size is proportional to the number of interactions. Src is a major node in the podocyte-specific interaction network. C-D. Comparison of cultured and native podocyte proteome. Overlap between this dataset and samples from cultured mouse podocytes (33°C, undifferentiated and 37°C, differentiated, samples previously published [Rinschen et al. AJP cell 2016, DOI:10.1152/ajpcell.00121.2016]) were compared. D. Intensities of the common proteins between the podocyte proteome and the previously acquired podocyte proteome were normalized and clustered using hierarchical clustering. 8 major clusters were defined.

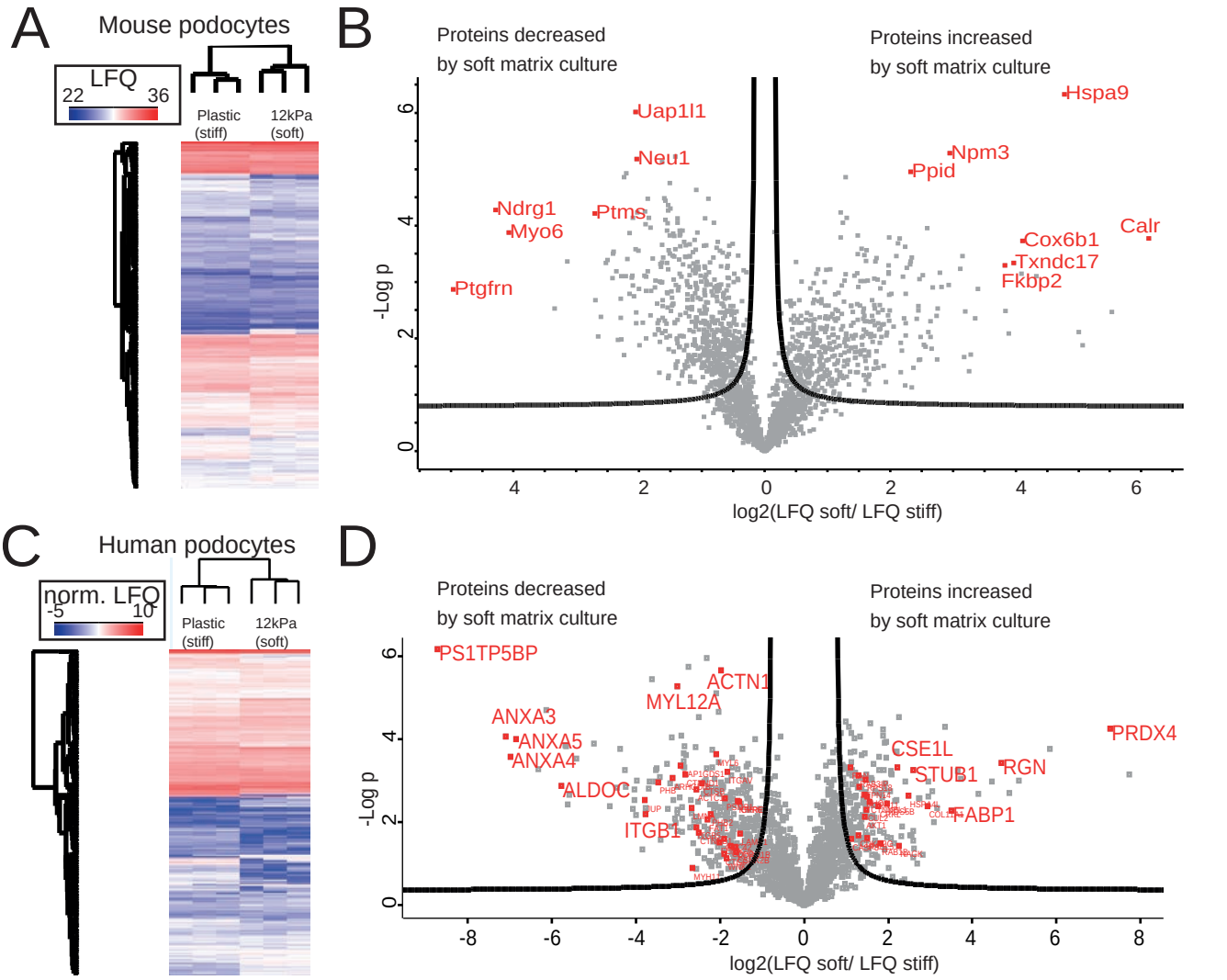
A
Mouse podocytes
LFQ
22
36
Plastic (stiff)
12kPa (soft)
B
Proteins decreased by soft matrix culture
Proteins increased by soft matrix culture
Uap1l1
Neu1
Ndrg1
Myo6
Ptms
Ptgfrn
Hspa9
Npm3
Ppid
Cox6b1
Calr
Txndc17
Fkbp2
-Log p
log2(LFQ soft/ LFQ stiff)
C
Human podocytes
norm. LFQ
-5
10
Plastic (stiff)
12kPa (soft)
D
Proteins decreased by soft matrix culture
Proteins increased by soft matrix culture
PS1TP5BP
ACTN1
MYL12A
ANXA3
ANXA5
ANXA4
ALDOC
ITGB1
CSE1L
STUB1
RGN
FABP1
PRDX4
-Log p
log2(LFQ soft/ LFQ stiff)
E
Proteins decreased with soft matrix
calcium binding
calcium-dependent phospholipid binding
cell-cell signaling
actin filament organization
cell-cell adhesion
actomyosin
actin filament bundle
stress fibers
mitochondrial inner membrane
protein-DNA complex
catenin complex
integrin complex
ENRICHMENT
F
Protein complexes decreased with soft matrix
WIPF1
MYL6
MYL12A
WAS
MYH9
ACTA2
t-test Difference_(1.500e-05
CDH2
JUP
PSEN1
CTNNB1
CDH1
t-test Difference_(9.836e-05
ITGB1
THBS1
ITGA3
t-test Difference_(1.342e-03
G
Proteins increased with soft matrix
damaged DNA binding
cellular aldehyde metabolic process
DNA-depndent DNA replicatin initiation
nucleus
cytosolic small ribosomal subunit
small ribosomal subunit
MCM complex
ENRICHMENT
H
Protein complexes increased with soft matrix
MCM7
MCMBP
MCM2
MCM3
MCM5
MCM6
MCM4
t-test Difference_(3.111e-04)
GAB1
SOS1
PTPN11
EGFR
CRK
CRKL
t-test Difference_(4.946e-02

Fig. S5

Fig. S5. Response of cultured podocytes to mechanical cues, Related to Fig. 4. A. Cultured mouse podocytes were seeded on plastic dishes (collagen coated) or on collagen coated “soft” matrix with defined elastic modulus (soft matrix, 12kPa). A proteomic profile of both groups was generated and hierarchical clustering of protein expression values was performed. B. Volcanoplot of protein quantification from podocytes on soft matrices as compared to podocytes on plastic dishes demonstrating significantly changed proteins. Proteins beyond the curved lines are significant based on FDR 0.05, s0= 0.1 C. Cultured human podocytes were seeded on plastic dishes (collagen coated) or on collagen coated “soft” matrix with defined elastic modulus (soft matrix, 12kPa). A proteomic profile was generated and hierarchical clustering of protein expression values was performed. D. Volcanoplot of protein quantification from podocytes on soft matrices as compared to podocytes on plastic dishes. E. GO-terms significantly overrepresented in proteins decreased on soft matrix. (FDR<0.05, Fishers exact test). F. Protein complexes significantly decreased on soft matrix. Protein complex enrichment analysis was performed using the COMPLEAT software for statistical overrepresentation in the dataset ($p<0.05$, corrected for multiple testing Bonferroni). G. GO-terms significantly overrepresented in proteins increased on soft matrix. (FDR<0.05, Fishers exact test). H. Protein complexes significantly decreased on soft matrix. Protein complex enrichment analysis was performed using the COMPLEAT software for statistical overrepresentation in the dataset ($p<0.05$, corrected for multiple testing).

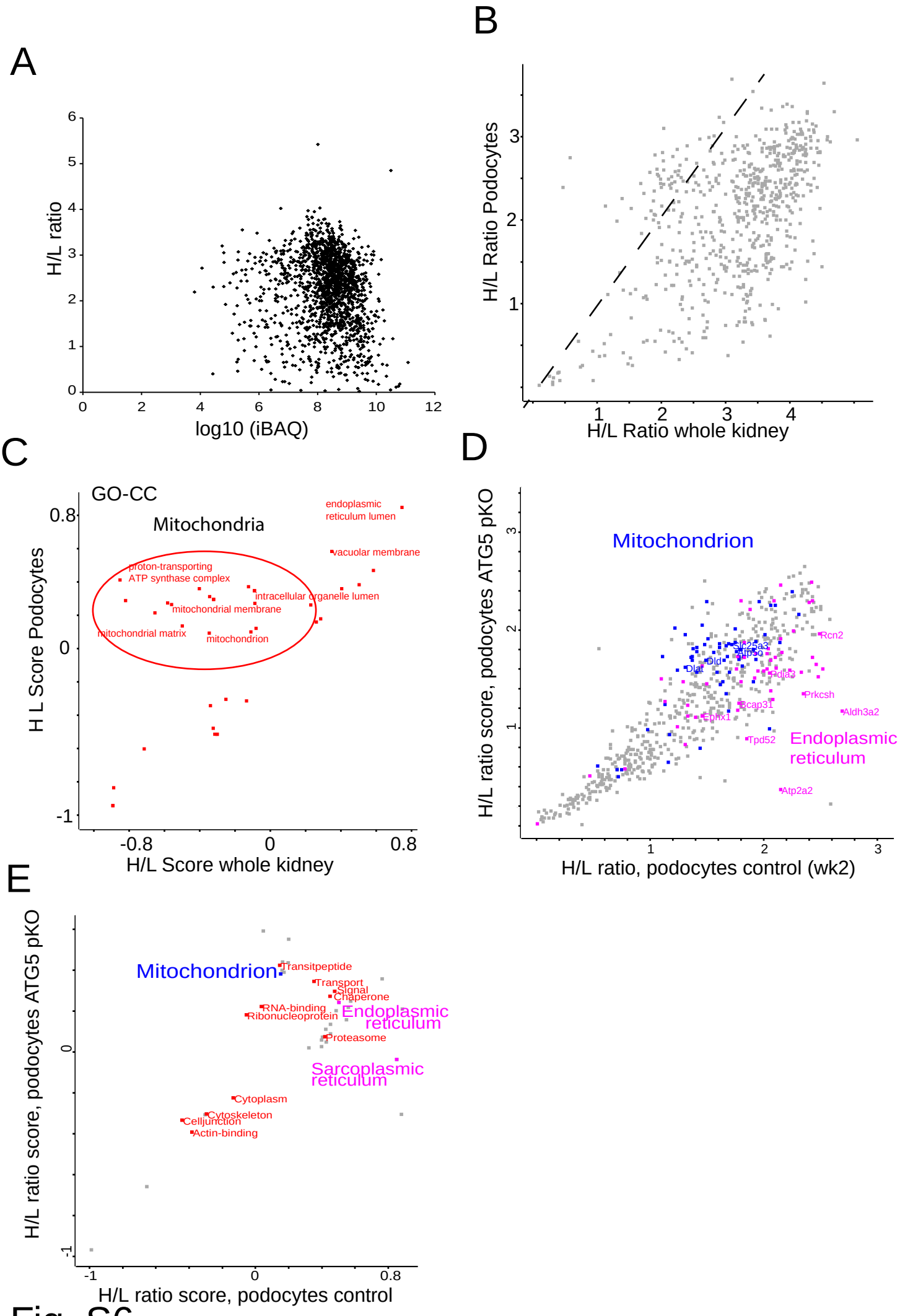
A
H/L ratio
log10 (iBAQ)
B
H/L Ratio Podocytes
H/L Ratio whole kidney
C
GO-CC
Mitochondria
endoplasmic reticulum lumen
vacuolar membrane
proton-transporting ATP synthase complex
intracellular organelle lumen
mitochondrial membrane
mitochondrial matrix
mitochondrion
H L Score Podocytes
H/L Score whole kidney
D
Mitochondrion
Endoplasmic reticulum
Rcn2
Slc25a3
Atp5o
Dld
Dlat
Pdia3
Prkcsh
Scap31
Aldh3a2
Ephx1
Tpd52
Atp2a2
H/L ratio score, podocytes ATG5 pKO
H/L ratio, podocytes control (wk2)
E
Mitochondrion
Transitpeptide
Transport
Signal
Chaperone
RNA-binding
Ribonucleoprotein
Endoplasmic reticulum
Proteasome
Sarcoplasmic reticulum
Cytoplasm
Cytoskeleton
Celljunction
Actin-binding
H/L ratio score, podocytes ATG5 pKO
H/L ratio score, podocytes control

Fig. S6

Fig. S6. Analysis of podocyte protein incorporation by pulsed in vivo stable isotope labeling, **Related to Fig. 5.** A. Scatter plot of heavy/light ratios and lg transformed iBAQ values demonstrating very weak negative correlation (R<-0.1). B. Scatter plot demonstrating H/L ratios in podocytes and whole kidney lysates. C. 2D enrichment analysis of Fig. S9B. Labeled dots determine significantly altered uniprot keyword terms (FDR < 0.05) D. Analysis of the effect of podocyte-specific ATG5 pKO on podocyte proteome as determined by pulsed stable isotope labeling in vivo. Scatterplot indicating H/L ratios in sorted podocytes of control and podocyte-specific ATG5 pKO mice after 2 weeks of feeding with stable isotope containing diet. E. 2D enrichment of Panel A (FDR<0.05). Labeled dots determine significantly altered uniprot keywords (FDR<0.05).

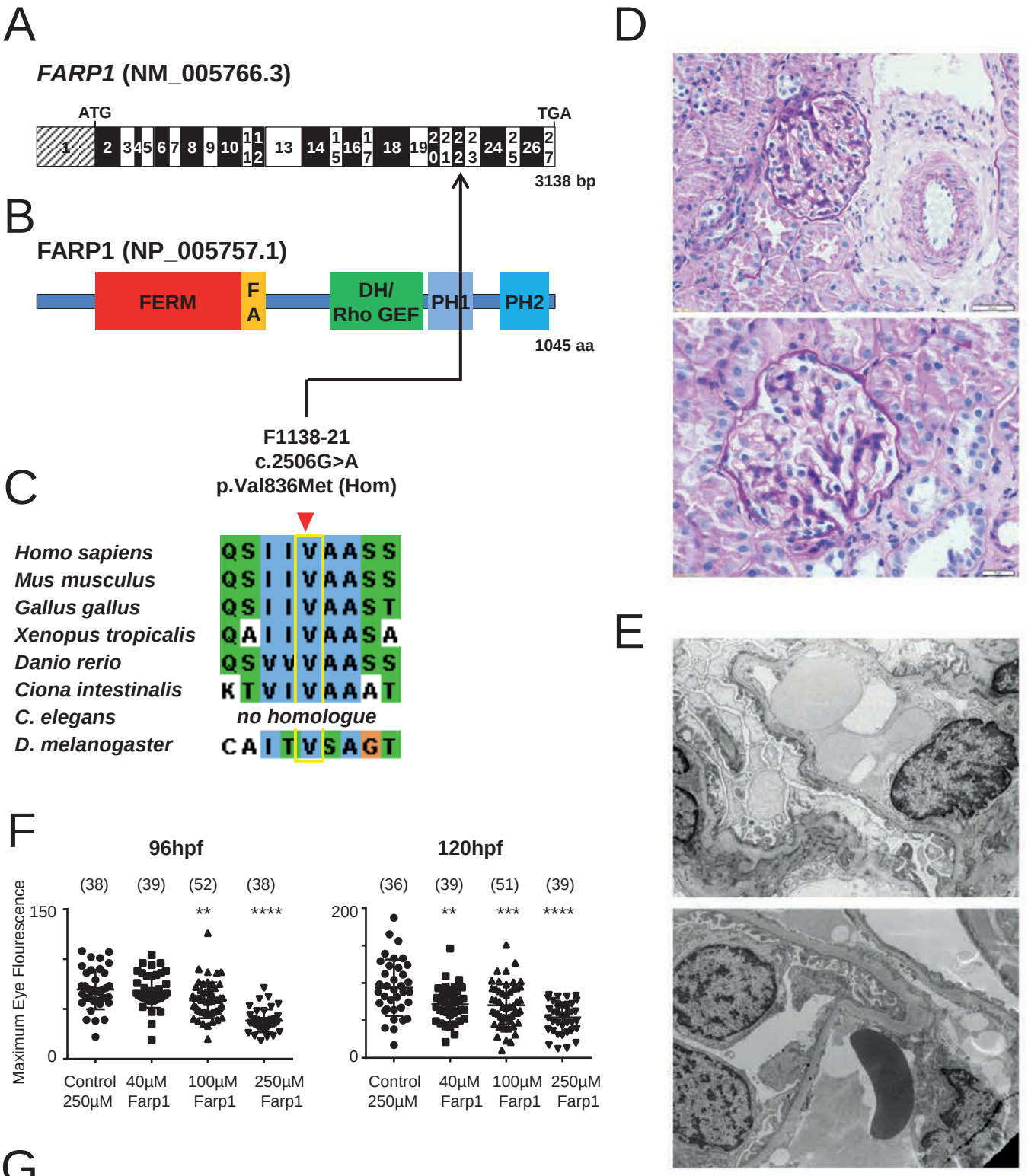
A
FARP1 (NM_005766.3)
ATG
TGA
3138 bp
B
FARP1 (NP_005757.1)
FERM
F A
DH/ Rho GEF
PH1
PH2
1045 aa
F1138-21
c.2506G>A
p.Val836Met (Hom)
C
Homo sapiens
Mus musculus
Gallus gallus
Xenopus tropicalis
Danio rerio
Ciona intestinalis
C. elegans
no homologue
D. melanogaster
D
E
F
96hpf
120hpf
Exp1
Maximum Eye Flourescence
(38) (39) (52) (38)
(36) (39) (51) (39)
Control 250μM
40μM Farp1
100μM Farp1
250μM Farp1
G
Phenotype number (%)
Phenotype severity
p1
p12
p2
p3
p4
Control 250uM
40uM Farp1
100uM Farp1
250uM Farp1

Fig. S7

Fig. S7. Whole exome sequencing identifies recessive mutations in the genes *FARP1* in a family with nephrotic syndrome, Related to Fig. 6. A. Exon structure of *FARP1* cDNA. Positions of start codon, stop codons, and mutated nucleotides are indicated. B. Domain structure of the proteins FARP1. Arrows indicate the positions of the mutated amino acid residues in families F1138 (FARP1). C. Evolutionary conservation amongst orthologous proteins of FARP1 (left). The mutated amino acid residue in family F1138 is indicated with arrowheads and a yellow box. D. Histology of renal biopsy of index patient showing focal segmental glomerulosclerosis. E. Electron microscopy of renal biopsy of index patient showing partial podocyte effacement. F. Analysis of proteinuria phenotype in zebrafish larvae. Morpholinos were injected into fertilized zebrafish eggs at one- to four-cell–stage. The transgenic zebrafish produce a vitamin D-binding protein GFP fusion protein with a size of 78kD. This protein accumulates in the circulation and is quantified 96 hpf and 120 hpf (hours past fertilization) by measuring the fluorescence level over the retina. Reduced fluorescence indicates a disturbed glomerular filtration barrier. Asterisks indicate significance in ANOVA vs control). Each dot corresponds to an individual larva, and total n numbers are depicted in brackets. G. Assessment of phenotype severity 120 hpf. The phenotype (degree of edema) was scored from P1 to P4 (with P1-2, P2 and P3 as intermediate scores, based on the amount of edema present in the yolk sac or the presence of pericardial effusion).

Supplemental Experimental Procedures

Glomerular isolation

We essentially used the same method as described previously(Boerries et al., 2013). Briefly, kidneys were dissected together with the abdominal aorta and transferred into dishes filled with 37°C prewarmed Hank's buffered salt solution (HBSS). Each kidney was perfused slowly through the renal artery with 2 ml 37°C bead solution and 0,5 ml bead solution plus enzymatic digestion buffer [containing: collagenase 300 U/ml (Worthington, Collagenase Type II, USA), 1 mg/ml pronase E (Sigma P6911, Germany) DNase I 50 U/ml (Applichem A3778, Germany)]. Kidneys were minced into 1 mm^3 pieces using a scalpel. After addition of 3 ml digestion buffer they were incubated at 37°C for 15 min on a rotator (100 rpm). The solution was pipetted up and down with a cut 1000 µl pipette tip every 5 min. After incubation all steps were performed at 4 °C or on ice. The digested kidneys were gently pressed twice through a 100 µm cellstrainer and the flow through was washed extensively with HBSS. After spin down, the supernatant was discarded and the pellet resuspended in 2 ml HBSS. These tubes were inserted into a magnetic particle concentrator and the separated glomeruli were washed twice.

Podocyte Preparation

Glomeruli were resuspended in 2 ml digestion buffer and incubated for 40 min at 37°C on a thermomixer shaking at 1400/min. During this incubation period the glomeruli were sheared with a 27 G needle at 15 min, and mixed by pipetting twice at 5, 10, 15, 20 and 25 min using a glass pipette. Podocytes were loosened at 10, 20, 30 min by vortexing once. After 40 min the solution was vortexed three times and the digestion result controlled by fluorescence microscopy. Samples were put on a magnetic particle concentrator again to eliminate beads and glomerular structures void of podocytes. The supernatant was pooled and the magnetic particles discarded. The cell suspension (2 ml) was sieved through a 40 µm pore size filter on top of a 50 ml Falcon tube, rinsed with 10 ml of HBSS. Cells were collected by centrifugation at 1500 rpm for 5 min at 4°C, resuspended in 0.5 ml of HBSS supplemented with 0.1% BSA plus DAPI (1 µg/ml). To separate GFP-expressing (GFP+) and GFP-negative (GFP-) cells, glomerular cells were sorted with a Mo-Flo cell sorter (Beckman Coulter) with a

Laser excitation at 488nm (Power 200 mW) and a sheath pressure of 60 PSI. Cells were kept at 4°C before entering the FACS machine and thereafter, while temperature during the sorting procedure (approx. 3 min) was 22°C. Only viable (DAPI negative) cells were sorted (laser excitation 380nm, power 80 mW). For the deep proteomics analysis on average 3,000,000 podocytes out of four mice (male, age 8-12 weeks) were pooled per biological replicate. For the RNASeq analysis the total RNA of nearly 12,000,000 podocytes and 19,000,000 non-podocyte glomerular cells (out of 29 mice, male, age 8-12 weeks) was used. For details on sample preparation and LC-MS/MS analysis see extended methods.

Sample preparation of podocytes for LC-MS/MS

For proteomic deep mapping, snap-frozen podocytes were dissolved in 8 M urea and 100 mM ammonium bicarbonate and lysates were generated. Protein lysates were sonicated (20 pulses, 0.1% power, 0.1s sonication cycle) and spun down at 4 degrees (16,000 g, 20min) to clear the debris. Supernatants were saved for further analysis. Protein concentration was determined using a commercial BCA assay (Thermo). 100 µg of protein were reduced with DTT (10 mM) and alkylated with iodoacetamide (40 mM) for 1h at room temperature in the dark, respectively. Podocytes were digested using trypsin at a 1:100 w/w ratio over night with shaking. The next day, ~25µg of peptides were fractionated using a six-layered SCX resin and fractionation using six different buffers as previously described: Six layered tips with SCX resin (Polystyrene-divinylbenzene copolymer modified with sulfonic acid) stage tips were conditioned with Acetonitrile (ACN) and washed with 0.2 % formic acid. Then, the supernatant was loaded on the in-tip columns and centrifuged until all of the peptide suspension passed the membrane. After washing the membrane of the stage tips with 0.2 % formic acid, 6 different cationic buffers with increasing concentrations of ammonium acetate were used to subsequently elute bound peptides: (SCX 1: 50 mM ammonium acetate (AA), 20% (v/v) ACN, 0.5% (v/v) formic acid (FA); SCX 2: 75 mM AA, 20% (v/v) ACN, 0.5% (v/v) FA; SCX 3: 125 mM AA, 20% (v/v) ACN, 0.5% (v/v) FA; SCX 4: 200 mM AA, 20% (v/v) ACN, 0.5% (v/v) FA; SCX 5: 300 mM AA, 20% (v/v) ACN, 0.5% (v/v) FA; Buffer X: 5% (v/v) Ammonium hydroxide, 80% (v/v) ACN). The flow through was collected for each of the six buffers separately during centrifugation. In the end, all the collected flow-through was dried down in a speedvac for 30 minutes at 30 °C. Subsequently peptides were stored at -20 °C until resuspension in 0.1% formic acid and subjection to nLC-MS/MS.

Bioinformatic analysis of deep proteomic data

For details on sample preparation and mass spectrometry analysis see extended methods. Raw files were analyzed using MaxQuant v 1.5.1.2 (Cox and Mann, 2008) and data was searched against a uniprot reference proteome for mouse or human downloaded at February 2014. MaxQuant options were default with match between runs enabled. The MaxQuant LFQ algorithm was enabled (Cox et al., 2014). Bioinformatic analysis was performed using Perseus v 1.5 (Cox and Mann, 2012). Briefly, reverse and contaminant hits were filtered out and proteins only identified by a site (site only) were removed. LFQ intensities were logarithmized, and a podocyte specific proteins were analyzed using a two-tailed t-test after imputation of missing values as described previously (Kohli et al., 2014). Correction for multiple testing was performed using an approach similar to SAM as initally published by Tusher et al. (Tusher et al., 2001). The parameters are detailed in the figure legends. Network analysis of podocyte-enriched proteins was performed using the netbox algorithm (Cerami et al., 2010) and default settings (p=0.05, maximal linker 2), using updated protein-protein interaction databases (3/2015) as input. The annotation of GO Terms was performed in Perseus 1.5.5.3 and a Fisher's exact test with correction for multiple testing (FDR<0.05) was utilized. The annotation of protein domains (both INTERPRO and PFAM domains) was performed in Perseus 1.5.5.3 and a Fisher's exact test with correction for multiple testing (FDR < 0.02) was performed. Enrichment was plotted vs –log (p value). mRNA seq raw values were matched on proteins using ENSEMBL identifiers, and 2D GO enrichment (FDR < 0.05) was performed. Multiple datasets were merged using ENSEMBL identifiers, and z-scored using perseus. The R package Rt-SNE was used for clustering. The raw data of the deep proteomic study is publically available via PRIDE (http://www.ebi.ac.uk/pride). PXD004040. Username: reviewer71610@ebi.ac.uk. Password: abpVHKL5. PXD005801. Username: reviewer36299@ebi.ac.uk. Password: QkntlstG.

RNA preparation and RNA sequencing

For RNA-Seq experiments isolated cells (Podocytes and Non-Podocytes glomerular cells) of 29 Gt(ROSA)$^{26Sortm4(ACTB-tdTomato,-EGFP)Luo/J}$ Tg(NPHS2-cre)295Lbh male mice at the age of 10 weeks were pooled. Under RNase-free conditions RNA was extracted with the chloroform/phenol method and DNase digested at the end of the preparation process. 15,5 µg non-podocyte and 19,2 µg podocyte

RNA were obtained. RNA quality control was performed as required by the RNASeq protocol. The Illumina (Illumina, San Diego, CA, USA) TruSeq stranded total RNA sample preparation LS protocol was used for directional, polyA+ library preparation. Sequencing was performed on a full flowcell of the HiSeq2500 sequencing machine using 100 cycles (Illumina, San Diego, CA, USA), with a depth of approximately 300M paired reads (600M total reads) and therefore approximately 150M paired reads per sample. Quality check was performed using FastQC 0.11.4 (Babraham Bioinformatics - FastQC A Quality Control tool for High Throughput Sequence Data.).

Analysis of mRNAseq data.

Pooled RNA of native mouse podocytes and non-podocytes glomerular cells was sequenced in two technical replicates. All RNA-Seq experiments were quantified using Salmon Beta 0.5.1 ((Patro et al., 2017)). RNA-Seq raw for quantification of published studies were downloaded from the European Nucleotide Archive (Toribio et al., 2017) please see Supplemental Table 3 for information about individual experiments ((Brunskill et al., 2014; Fu et al., 2016; Kann et al., 2015; Lin et al., 2014; Pervouchine et al., 2015)).

In general, analysis of transcriptomic data was performed using the R statistical software package (R Core Team (2016). R: A language and environment for statistical computing. R Foundation for Statistical Computing, Vienna, Austria. URL: https://www.R-project.org/.) as well as specific packages provided by Bioconductor (Huber et al., 2015) Graphical Plotting (Principal component, Scree plot, heat plot, histogram) was done with the help of the ggplot2 package (ggplot2 - Elegant Graphics for Data Analysis | Hadley Wickham | Springer.). Differential expression analysis was performed using sleuth version 0.28.0 using a wald test (Pimentel et al., 2017). For Reactome (Croft et al., 2014; Milacic et al., 2012) analysis ReactomePA (Yu and He, 2016) and clusterProfiler package (Yu et al., 2012) Bioconductor package was used on significantly regulated transcripts ($q < 0.001$ & $b > 1.5$) (accessed 9/2016). Raw data were deposed at EBI Array Express with experiment accession number E-MTAB-5457 (Username: Reviewer_E-MTAB-5457, Password: KC158Tch). Podocyte specificity was calculated as a ratio of tpm(Podocyte)/sum tpm (all other tissues). RNAseq datasets from other tissues were derived from the mouse RNA Profiling datasets by the ENCODE

project, using the datasets SRR453077-SRR453175; SRR567478- SRR567503, all processed in an identical fashion.

Drosophila experiments

D. melanogaster stocks were cultured on standard cornmeal molasses agar food and maintained at 25°C. RNAi-Based Nephrocyte Functional Screen Procedure: Virgins from MHC-ANF-RFP, HandGFP, and Dot-Gal4 transgenic lines (Gift from Zhe Han, University of Michigan, Ann Arbor, USA) were crossed to UAS-CG9093-RNAi (VDRC TID 9696/GD) males at 25°C; 2 days after crossing, flies were transferred to small collection cages with grape juice agar plates to collect the embryos for 24 hours at 25°C. Collected embryos were aged for 48 hours at 29° C and then subjected to examination of the RFP accumulation in pericardial nephrocytes using a confocal microscope. The RFP mean fluorescence intensity of GFP positive areas was measured to quantify the uptake efficiency. The result was verified using a second RNAi (VDRC 101473/KK). For transmission electron microscopy Virgins of prospero-Gal4 (gift from Barry Denholm, University of Edinburgh, Edinburgh, UK) were crossed to UAS-CG9093-RNAi (VDRC TID 9696/GD) for a garland cell-specific knockdown of Tsp26A. Drosophila garland cells were freshly prepared and immerse fixed for three days at 4°C using 4% paraformaldehyde plus 1% glutaraldehyde (Sigma Aldrich, Germany; in 0.1M PB buffer, pH 7.4) as a fixative. The samples were contrasted using 1% osmiumtetroxide (Roth, Germany; 30 min at RT) and 1% uranylacetate (30 min at RT in 70% ethanol), dehydrated stepwise and finally embedded in epoxy resin (Durcopan, SimgaAldrich, Germany). Ultrathin sections were cut using a Leica Ultracut 6. Section imaging and analysis was performed using a Philipps CM10 TEM.

Sample preparation for proteomic analysis of cell culture experiments.

Cells were harvested by scraping in 8M urea and 100mM Ammonium bicarbonate on ice with 1x protease/phosphatase inhibitor. Then, proteins were reduced (5 mM DTT at room temperature for 1h), and alkylated (10mM IAA at room temperature for 1h in the dark). The proteins (~50 µg as determined by a BCA assay [Thermo]) were digested using a 1:100 trypsin/protein ratio over night at room temperature. The next day, peptide solution was acidified and subjected to Stage tip cleanup as

above described (Rappsilber et al., 2003) and mass spectrometry analysis on a Q Exactive plus machine as previously described (2.5 h gradient). For details on bioinformatics analysis, please see supplementary methods.

Bioinformatic analysis of cell culture experiments

Raw data was processed with MaxQuant and intensities were logarithmized, contaminants were removed and raw data was normalized by substraction of the mean. Data were uploaded in perseus and hierarchical clustering (based on Euclidean distance) was performed. Imputation was performed for at least 4/6 valid values. COMPLEAT (Vinayagam et al., 2013) algorithm was utilized to determine regulated protein complexes in human podocytes. The log2 ratio of LFQ (con/12kPA) was utilized as software input with default settings (accessed 12/2016). GO terms and uniprot keywords were annotated in perseus (v. 1.5.5.3) (Tyanova et al., 2016) and category enrichment was performed by a Fisher's exact test (FDR controlled with FDR <0.05). Data was extracted from the human protein atlas in February 2015 and converted into mouse gene symbols using NCBI homologene groups (release 3/2015), which were then matched on the dataset.

Pulsed in vivo stable isotope labeling

Stable isotope labeling of animals was performed as previously described by Krueger et al. (Krüger et al., 2008) Lys(0)-SILAC-Mouse control ($^{12}C_6$-lysine) and Lys(6)-SILAC-Mouse SILAC ($^{13}C_6$-lysine, 97 %) mouse diet was purchased from Silantes, Martinsried, Germany. Mice in SILAC feeding experiments were kept isolated in single individual cages with metal grids. Initially Mice were fed 3 g daily of Lys(0)-SILAC-Mouse control diet for 3 weeks. Afterwards they were switched to 3 g daily Lys(6)-SILAC-Mouse SILAC diet for 1, 2 or 3 weeks according to the experimental protocol and sacrificed afterwards for glomerular isolation. Please see Supplemental table 14+15 for additional details of mice used for this study. The data presented are the average of at least 2 biological replicates for podocytes (for three different timepoints) and kidney tissue.

Sample preparation and proteomics of in vivo stable isotope labeled tissue

SILAC mice and kidneys were perfused and podocytes were isolated exactly as described above. Then, snap-frozen podocytes were lysed in SDS and fractionated using 1D Gel electrophoresis and processed as previously described in gel-with 6-10 gel pieces/protein (Boerries et al., 2013). The digestion was performed with LysC (w/w ratio of 1:10). Analysis of pulsed SILAC labeled podocytes was performed using an LTQ Orbitrap XL mass spectrometer coupled to a nLC as previously described (Boerries et al., 2013).

Bioinformatic analysis of dynamic proteomic data

Proteomics data were searched with MaxQuant v 1.4.1.2 against an UNIPROT mus musculus database downloaded on March 2016. Multiplicity was set to 2 (with Lysine + 6 Da), and the maximal number of labeled amino acids was 4. The protease was LysC/P, with three maximal missed cleavages. Minimum peptide length was 7, variable modifications were methionine oxidation and protein N-terminal acetylation. Carbamidomethylcysteine was set as fixed modification. MatchBetweenRun option was not enabled. The non-normalized ratios were used for further procedures. The resulting ratios were merged using Perseus und filtered for reverse, contaminant and "site only" proteins Then, the resulting matrix was filtered so only valid ratios were obtained. 2D GO enrichment analyses were applied as described above. H/L ratios were normalized using the following term depicting the "number of heavy amino acids", using the iBAQ obtained from Fig. 1 and using the amino acid copy numbers obtained from uniprot for the leading majority protein. The following formula was used to correct ratios:

$$n(heavy\ amino\ acids) = incorporation\ rate * n(amino\ acids\ per\ protein) * n(protein\ copies)$$

$$= \frac{H/L}{H/L + 1} * n\ (amino\ acids\ per\ protein) * iBAQ$$

In situ hybridization

Mouse isolated podocyte RNA served to clone fragments of 5′-UTR and coding sequence of mouse *Farp1* using the One-Step PCR Kit (Qiagen, Heidenheim, Germany). PCR fragments were

inserted into a modified *pBluescript (KS-)* vector (Invitrogen, Carlsbad, CA) using *NotI* and *MluI* restriction sites. *pBluescript* Vector was linearized and digoxigenin-(DIG)-labeled antisense riboprobes were generated using T7-RNA-polymerase (Roche, Mannheim, Germany). For paraffin section ISH, slides were progressively rehydrated. After prehybridization (20 min), hybridization with DIG-UTP probes took place overnight in standard hybridization buffer (SSC pH 4.5; containing deionized 50% formamide, 1% SDS, heparine 50µg/ml and yeast RNA 50µg/ml) at 60 °C. Specimens were then incubated with alkaline phosphatase-conjugated anti-DIG Fab fragments (Roche, Mannheim, Germany) at a dilution of 1:3000 for 2 h at room temperature. Alkaline phosphatase was detected using chromogenic conversion of BM Purple (Roche). Slides were then progressively dehydrated in xylol, counterstained with Eosin and mounted. The following primers were used:

Farp1(based on NM_028734.5)

ISH FARP1 449 fp 5'-CGCGGGACGCGTTGGAACGAGGACAGAAACCA -3'

ISH FARP1 1445 rp 5'- CGCGGGGCGGCCGCTTGTGGCCGCCTTCTTTAAC-3';

Multi-omics candidate gene list, whole exome sequencing, multi gene-panel testing and mutation calling.

To obtain a candidate list of genes we performed clustering analysis of z-normalized relative mRNA expression levels, relative protein expression levels, absolute protein expression levels as well as tissue specificity of the podocyte mRNA levels. We found that disease-associated genes in slit diaphragm and actin-related processes were largely defined by very high z-scores in all four parameters, and clustered in close proximity. Ranking individual genes based on their scores in each parameter, combined with additional information from the human protein atlas, glomerular disease datasets (www.nephromine.org), as well as importance of the respective gene in go-term analysis generated a list of 280 candidate gene-protein pairs. To test these in patient cohorts, we performed different next-generation sequencing (NGS) based approaches. First, we performed whole exome sequencing (WES) using Agilent SureSelect™ human exome capture arrays (Thermo Fisher Scientific) with NGS on an Illumina™ platform. Sequence reads were mapped against the human reference genome (NCBI build 37/hg19) using CLC Genomics Workbench (version 6.5.1) (CLC bio).

Mutation calling was performed in line with proposed guidelines by scientists, who had knowledge of clinical phenotypes, pedigree structure, and genetic mapping. 430 families with nephrotic syndrome were screened for mutations in 280 candidate genes derived from the “multi-omics” approach. Families with mutations in genes known to cause nephrotic syndrome, if mutated, were excluded from the study. Second, all exons and adjacent intronic boundaries of a different number of genes (dependent on the version of our customized multi-gene panel, including *FARP1*) known or hypothesized to cause nephrotic syndrome and related phenotypes were targeted by a custom SeqCap EZ choice sequence capture library (NimbleGen, Madison, Wisconsin, USA) and subsequently sequenced on an Illumina MiSeq or HiSeq platform (2x150 PE) according to the manufacturer´s protocol. A total of 700 patients were analyzed with an average coverage of 120-fold (MiSeq) or more than 200-fold (HiSeq), respectively. Bioinformatic analysis was performed as recently described.

Zebrafish experiments

Transgenic zebrafish Tg(l-fabp:DBP-EGFP) were a kind gift from B. Anand-Apte, Cleveland, OH (Xie et al., 2010). They were grown and mated at 28.5° C and embryos were kept and handled in standard E3 solution as previously described (Hentschel et al., 2007). Morpholino sequence for farp1 was 5'UTR: GTGTCTTTAAATGATATTCCGCTGG, for control: CCTCTTACCTCAGTTACAATTTATA. They were injected in one- to four-stage embryos using a Nanoject II injection device (Drummond Scientific, Broomall, PA). Morpholinos were ordered from GeneTools (Philomath, OR). Injections were carried out in injection buffer (100 mM KCl, 0.1% phenol red) and at 48 hours post fertilization (hpf) remaining chorions were manually removed. Edema assessment and fluorescence based eye assays were performed as previuously described (Hanke et al., 2013). The animal protocol was approved by the MDI Biological Laboratory IACUC (#11-02).

Supplemental References

Bartram, M.P., Habbig, S., Pahmeyer, C., Höhne, M., Weber, L.T., Thiele, H., Altmüller, J., Kottoor, N., Wenzel, A., Krueger, M., et al. (2016). Three-layered proteomic characterization of a novel ACTN4 mutation unravels its pathogenic potential in FSGS. Hum. Mol. Genet.

Boerries, M., Grahammer, F., Eiselein, S., Buck, M., Meyer, C., Goedel, M., Bechtel, W., Zschiedrich, S., Pfeifer, D., Laloë, D., et al. (2013). Molecular fingerprinting of the podocyte reveals novel gene and protein regulatory networks. Kidney Int. *83*, 1052–1064.

Brunskill, E.W., Park, J.-S., Chung, E., Chen, F., Magella, B., and Potter, S.S. (2014). Single cell dissection of early kidney development: multilineage priming. Dev. Camb. Engl. *141*, 3093–3101.

Croft, D., Mundo, A.F., Haw, R., Milacic, M., Weiser, J., Wu, G., Caudy, M., Garapati, P., Gillespie, M., Kamdar, M.R., et al. (2014). The Reactome pathway knowledgebase. Nucleic Acids Res. *42*, D472-477.

Fu, J., Wei, C., Lee, K., Zhang, W., He, W., Chuang, P., Liu, Z., and He, J.C. (2016). Comparison of Glomerular and Podocyte mRNA Profiles in Streptozotocin-Induced Diabetes. J. Am. Soc. Nephrol. JASN *27*, 1006–1014.

Hanke, N., Staggs, L., Schroder, P., Litteral, J., Fleig, S., Kaufeld, J., Pauli, C., Haller, H., and Schiffer, M. (2013). “Zebrafishing” for novel genes relevant to the glomerular filtration barrier. BioMed Res. Int. *2013*, 658270.

Hentschel, D.M., Mengel, M., Boehme, L., Liebsch, F., Albertin, C., Bonventre, J.V., Haller, H., and Schiffer, M. (2007). Rapid screening of glomerular slit diaphragm integrity in larval zebrafish. Am. J. Physiol. Renal Physiol. *293*, F1746-1750.

Huber, W., Carey, V.J., Gentleman, R., Anders, S., Carlson, M., Carvalho, B.S., Bravo, H.C., Davis, S., Gatto, L., Girke, T., et al. (2015). Orchestrating high-throughput genomic analysis with Bioconductor. Nat. Methods *12*, 115–121.

Kann, M., Ettou, S., Jung, Y.L., Lenz, M.O., Taglienti, M.E., Park, P.J., Schermer, B., Benzing, T., and Kreidberg, J.A. (2015). Genome-Wide Analysis of Wilms’ Tumor 1-Controlled Gene Expression in Podocytes Reveals Key Regulatory Mechanisms. J. Am. Soc. Nephrol. JASN *26*, 2097–2104.

Krüger, M., Moser, M., Ussar, S., Thievessen, I., Luber, C.A., Forner, F., Schmidt, S., Zanivan, S., Fässler, R., and Mann, M. (2008). SILAC mouse for quantitative proteomics uncovers kindlin-3 as an essential factor for red blood cell function. Cell *134*, 353–364.

Lin, S., Lin, Y., Nery, J.R., Urich, M.A., Breschi, A., Davis, C.A., Dobin, A., Zaleski, C., Beer, M.A., Chapman, W.C., et al. (2014). Comparison of the transcriptional landscapes between human and mouse tissues. Proc. Natl. Acad. Sci. U. S. A. *111*, 17224–17229.

Milacic, M., Haw, R., Rothfels, K., Wu, G., Croft, D., Hermjakob, H., D’Eustachio, P., and Stein, L. (2012). Annotating cancer variants and anti-cancer therapeutics in reactome. Cancers *4*, 1180–1211.

Patro, R., Duggal, G., Love, M.I., Irizarry, R.A., and Kingsford, C. (2017). Salmon provides fast and bias-aware quantification of transcript expression. Nat. Methods *14*, 417–419.

Pervouchine, D.D., Djebali, S., Breschi, A., Davis, C.A., Barja, P.P., Dobin, A., Tanzer, A., Lagarde, J., Zaleski, C., See, L.-H., et al. (2015). Enhanced transcriptome maps from multiple mouse tissues reveal evolutionary constraint in gene expression. Nat. Commun. *6*, 5903.

Pimentel, H., Bray, N.L., Puente, S., Melsted, P., and Pachter, L. (2017). Differential analysis of RNA-seq incorporating quantification uncertainty. Nat. Methods *14*, 687–690.

Toribio, A.L., Alako, B., Amid, C., Cerdeño-Tarrága, A., Clarke, L., Cleland, I., Fairley, S., Gibson, R., Goodgame, N., Ten Hoopen, P., et al. (2017). European Nucleotide Archive in 2016. Nucleic Acids Res. *45*, D32–D36.

Xie, J., Farage, E., Sugimoto, M., and Anand-Apte, B. (2010). A novel transgenic zebrafish model for blood-brain and blood-retinal barrier development. BMC Dev. Biol. *10*, 76.

Yu, G., and He, Q.-Y. (2016). ReactomePA: an R/Bioconductor package for reactome pathway analysis and visualization. Mol. Biosyst. *12*, 477–479.

Yu, G., Wang, L.-G., Han, Y., and He, Q.-Y. (2012). clusterProfiler: an R package for comparing biological themes among gene clusters. Omics J. Integr. Biol. *16*, 284–287.

Babraham Bioinformatics - FastQC A Quality Control tool for High Throughput Sequence Data.

ggplot2 - Elegant Graphics for Data Analysis | Hadley Wickham | Springer.